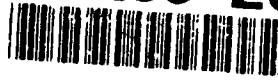AFIT/GAE/ENY/92D-02

FATIGUE BEHAVIOR OF A CROSS-PLY
CERAMIC MATRIX COMPOSITE UNDER TENSION-
TENSION AND TENSION-COMPRESSION LOADING

THESIS

Frank A. Opalski
Captain, USAF
AFIT/GAE/ENY/92D-02

DTIC

S
JAN 1 1 1993
D

93-00140

FATIGUE BEHAVIOR OF A CROSS-PLY

CERAMIC MATRIX COMPOSITE UNDER TENSION-

TENSION AND TENSION-COMPRESSION LOADING

THESIS

Presented to the Faculty of the School of Engineering

of the Air Force Institute of Technology

Air University

In Partial Fulfillment of the

Requirements for the Degree of

Master of Science in Aeronautical Engineering

Frank A. Opalski

Captain, USAF

December 1992

Approved for public release; distribution unlimited

Accession For

NTIS GRA&I	☑	
DTIC TAB	☐	
Unannounced	☐	
Justification		

By

Distribution/

Availability Codes

	Avail and/or
Dist	Special
A-1	

Preface

The primary purpose of this study was to investigate the room-temperature fatigue response and failure mechanisms of Nicalon/CAS, a fiber-reinforced ceramic matrix composite, under tension-compression loading. Initial tests identified the static behavior of the composite in tension and compression. Subsequent tests then verified the tension-tension and compression-compression characteristics. Final tests determined the effects that tension-compression loading produced.

While many individuals were of great assistance in this project, foremost and without a doubt was my advisor Dr. Shankar Mall. His knowledge, patience, understanding and guidance were the key ingredients for my success. My thanks also extend to my committee members, Lt. Col. Ronald Bagley and Dr. Anthony Palazotto, who provided additional feedback and support in this undertaking.

I must also recognize the AFIT laboratory personnel for their superb efforts to have supplies on hand and equipment readily available and working. My appreciation goes to Jay Anderson, Andy Pitts, Dan Rioux, and especially to Mark Derriso, who must have heard my nagging every day and always provided materials and equipment in a timely manner.

Thanks are also necessary for Joe Hoffle from the AFIT Model Shop who provided me with numerous machined parts for the test station; Bob Lewis, Eric Fletcher and Mike Scott from the Materials Directorate, Wright Laboratory, whose assistance in polishing and micro-photography was a tremendous aid; Dr. Larry Zawada and Capt. John Pernot, also from the Materials Directorate, for their knowledge about ceramic composites; and the Air Force Office of Scientific Research (AFOSR).

Finally, this thesis, as well as the entire AFIT Masters program, while long and demanding, has been unquestionably benefical and rewarding. I must, in conclusion, thank my wife Christine for her patience during these past eighteen months for putting up with me.

Table of Contents

List of Figures and Tables

Table #

Abstract

The purpose of this study was to investigate the behavior of a cross-ply ($[0/90]_{2s}$) Nicalon/Calcium-Aluminosilicate (Nicalon/CAS) ceramic matrix composite at room temperature under tension-compression fatigue loading. The primary objectives were to determine the threshold for which cycle runout (fatigue life of at least 1,000,000 cycles) would occur under tension-tension loading and then investigate the effects, if any, that tension-compression loading would produce.

The average value of the initial elastic modulus for this composite was 120 GPa in both tension and compression. Ultimate tensile strength was 275 MPa while ultimate compressive strength was 503 MPa. Tension-tension tests with a load ratio R ($R = \sigma_{min}/\sigma_{max}$) of 0.1 were accomplished at maximum stresses of 180, 160, and 140 MPa with cycles to failure of 1,609, 50,443, and cycle runout (1,000,000), respectively. In the 140 MPa test, transverse cracks (perpendicular to the load) developed within the first cycle in both the 0° and 90° plies. Transverse crack density increased slightly up to 10,000 cycles then remained relatively constant through 1,000,000 cycles.

With 140 MPa as the maximum tensile stress, tests with load ratios of -2.0, -1.5, and -1.0 were completed with cycles to failure of 10,816, 350,330 and cycle runout, respectively. In each case, transverse cracks formed during the first cycle as in the tension-tension tests. The transverse crack density gradually increased, then longitudinal cracks (parallel to the load) developed. These longitudinal cracks formed in the middle two 90° plies first, then additional longitudinal cracks formed in the same plies as well as in the outer 90° plies. Longitudinal crack length eventually spanned the entire specimen length. Failure occurred in compression with visible signs of delamination and micro-buckling.

Acetate replications were used to document crack growth. Stress-strain curves were recorded from which elastic modulus measurements were

made. In both tension-tension and tension-compression tests, most damage occurred during the first few cycles with the elastic modulus usually levelling off within a few thousand cycles to about thirty to fifty percent of its original value. The area under the stress-strain curves was calculated which provided an energy/volume value. This hysteretic energy value was always highest during the first cycle. It gradually decreased and then either remained relatively constant for the remainder of tests in which cycle runout occurred, or it began increasing for those tests where failure occurred. Thus, this energy calculation could be used to reasonably predict if specimen failure would occur.

Overall, tension-tension specimens achieved cycle runout as long as the maximum stress was at or below 140 MPa. Above this threshold, crack bifurcation in the 90° plies began occurring and transverse crack density in the 0° plies began rapidly increasing. For a constant maximum stress of 140 MPa, the addition of compression cycles was highly detrimental in that longitudinal cracks developed which ultimately led to specimen failure depending on the magnitude of the compressive load.

FATIGUE BEHAVIOR OF A CROSS-PLY CERAMIC

MATRIX COMPOSITE UNDER TENSION-TENSION AND

TENSION-COMPRESSION FATIGUE LOADING

I. Introduction

A. Background

For most of the twentieth century, ceramic materials have been associated with items like flower pots, vases, dishes, and various other household items. Their thermal capabilities allowed them to withstand high temperatures in ovens and kilns, and their low density made for relatively easy handling; however, low fracture toughness and ductility, i.e., brittleness, required delicate handling and low loading in order to prevent cracking and total fracture.

With the addition of high-strength reinforcing fibers like carbon and silicon carbide, the overall strength of the ceramic, as well as its fracture toughness, can be significantly increased. Depending on the application, the orientation of the fibers in the ceramic can be varied to obtain optimum performance. The addition of fibers to a ceramic is the creation of a ceramic matrix composite (CMC).

Because of their ability to withstand higher temperatures, the study of CMC's and their potential uses have been gradually increasing. In general, the higher the operating temperature achieved in engines, the greater the engine efficiency and overall performance. Consequently, CMC automobile engines which require no liquid cooling are currently being developed. In jet engines, CMC fan blades, nozzles, and combustion chamber components are already being tested. In high performance space vehicles like the space shuttle and the National Aerospace Plane, CMC's are being analyzed for use as fuselage panels.

Items such as engines, automobiles, and aircraft are all designed to operate with high reliability and provide years of continued use. They

1

are not one-shot devices like ammunition or solid-propellant rocket motors which are used once and then "thrown away." Therefore, their fatigue behavior must be known. This behavior is dependent on the type of loads that will be imposed on these items in their lifetime. An aircraft, for example, might have a flight profile which includes taxi, take-off, climb, cruise, air refueling, aerial maneuvering, descent, and landing. Each of these stages creates certain loads on the aircraft. In addition, this profile may be repeated daily for twenty years. Obviously, determining the behavior during one flight is needed but, more importantly, the effects that continued flights produce is of greater significance.

With this in mind, the need for fatigue testing becomes much more clear. The type of fatigue testing required, however, is not necessarily as obvious. Going back to the aircraft's flight profile, each stage will produce certain loads on the airframe. Some will yield positive stresses while certain other maneuvers may result in negative ones, or even both. The engine exhaust nozzle, with its opening and closing, will experience tension and compression loads, while the engine fan blades will most likely only see tension loads. Various other components will probably see some sort of combination of positive and negative loads.

Previous fatigue testing on ceramic matrix composites has focused primarily on tension-tension and compression-compression loading. Since there are limited studies on tension-compression testing, and the need to understand the behavior under tension-compression loading will eventually be required, it to investigate the effects of tension-compression fatigue loading that this study has been accomplished.

B. Problem Statement/Scope

The purpose of this study was to investigate the room-temperature (23° Celsius average) effects of tension-compression fatigue loading on a silicon fiber (Nicalon) reinforced calcium-aluminosilicate ceramic matrix composite.

2

C. Approach

A Nicalon/CAS ceramic matrix composite plate was cut into test specimens 7.62 cm long and 6.35 mm wide. These specimens were then tested on an MTS test station under various stresses and load ratios. Static tension and compression tests were initially performed to identify the static failure mechanisms. Tension-tension fatigue tests were completed which determined the threshold at which cycle runout occurred. Tension-compression tests were then run to identify the effects that compression cycles produced in the ceramic matrix composite.

Load and displacement data were recorded logarithmically for each fatigue test (cycles 1,2,5,10,20,50,100,200,...,1,000,000). Material behavior and damage was recorded by four primary methods: stress-strain curves, elastic modulus, hysteretic energy densities, and acetate replication techniques.

Elastic modulus measurements were made from each stress-strain curve. Only the initial loading portion of the curve was used. Reduction in the modulus with respect to the number of cycles indicated material damage had developed during fatigue loading.

Hysteretic energy dissipated during a fatigue cycle was calculated from the stress-strain curves. The area under these curves was found by summing a series of trapezoids which yielded an energy/volume value. These energy values indicated an increase in damage during cycling.

Since most cracks were not visible unless the specimen was under load, replicas were taken for each type of test. These replicas showed the crack development and progression as the cycle count increased.

Systematic investigation of damage mechanisms was made by using each of the above methods. These results were compared to substantiate and explain the observed fatigue behavior and the effects of the compression loading.

II. Background

A. Experimental Background

While ceramic matrix composites are relatively new, several studies have nevertheless been completed describing the behavior under various loading conditions. The static tensile behavior has been documented in numerous instances. While important, the fatigue behavior is more significant since materials are usually designed to last for years, not just for one cycle. The tension-tension behavior of ceramic composites is also well established; however, data on the tension-compression behavior is extremely limited.

Rousseau [1] described the sequence of crack progression in a cross-ply Nicalon/CAS specimen in various stages. The 90° plies first tended to lose their load carrying ability with the development of transverse cracks. This transverse matrix cracking then occurred in the 0° plies, followed by fiber breakage in the 0° plies. Ultimate strength, depending on lot, ranged up to 275 MPa.

Mall, Fink, and Kim [2] had also identified this transverse cracking in unidirectional specimens of Nicalon/CAS in both 0° and 90° layups. Mall and Kim [3] duplicated the transverse cracking sequence in a cross-ply Nicalon/CAS layup.

Zawada, Butkus, and Hartman [4] had tested SiC/1723 and specifically identified two distinct proportional limits corresponding to 90° ply matrix cracking followed by 0° ply matrix cracking. Wang and Parvizi-Majidi [5] had experimented with cross-ply Nicalon/CAS and varied the number of plies. They theorized that the number of plies affected when the transverse cracking in the 0° plies initiated.

For tension-tension testing, Rousseau had observed damage in the cross-ply Nicalon/CAS similar to that in the static tension tests. He concluded that the majority of damage occurred during the first load cycle. He also believed that the large elastic modulus stiffness loss

4

during the first cycle was not a uniquely cyclic phenomenon. Zawada, Butkus, and Hartman noted in SiC/1723 that loss of stiffness occurred during cyclic loading even below the proportional limits previously calculated.

Highsmith, Stinchcomb, and Reifsnider [6] had shown the development of a "Characteristic Damage State" (CDS) which depended only on the material properties. They concluded that matrix cracks in off-axis plies did not develop in a random manner but rather occurred uniformly based on the ability of the surrounding plies to transfer load into the cracked plies.

The availability of information on tension-compression testing of ceramic composites is very limited. Zawada and Pernot [7] investigated the tension-compression fatigue behavior of SiC/1723 at room temperature. They concluded that tension-compression cycling resulted in continual damage accumulation with the development of cracks growing parallel to the loading direction which reduced the overall fatigue life.

Rotem and Nelson [16] had analyzed the tension-compression fatigue behavior of both a unidirectional and a cross-ply graphite/epoxy composite. They observed the primary failure mode for both lay-ups occurs in compression. They concluded this was the result of the splitting of fiber bundles, ply delamination and subsequent buckling.

B. Models and Predictions

Throughout this study, the change in elastic modulus has been associated with material damage. The value of identifying the modulus and any reduction was explained by Reifsnider and Stinchcomb [6]. They developed a "Critical Element" approach which could be used to predict residual fatigue life. This approach focused on identifying the critical, life-limiting components of the composite. In this Nicalon/CAS composite, the critical components are the 0° plies, meaning as long as these do not fail, the specimen also should not fail. This approach was used in the

5

Total Discount Method of Classical Laminated Plate Theory by applying it to the 90° plies.

While there are currently no models available which accurately predict the fatigue life of ceramic matrix composites, the application of Classical Laminated Plate Theory (CLPT) can be used to reasonably estimate various laminate properties and failure stresses/strains. In order to do this, the material properties of a unidirectional Nicalon/CAS composite are required.

For Nicalon/CAS, Mall, Fink, and Kim [2] had calculated the values shown in Table 1 for the unidirectional composite:

<div align="center">

Table 1

Longitudinal Modulus E_1	139 GPa
Transverse Modulus E_2	93 GPa
In-Plane Shear Modulus G_{12}	42 GPa
Major Poisson's Ratio ν_{12}	0.25

</div>

The components of the stiffness matrix $[Q]$ can be expressed in terms of these engineering constants:

$$Q_{11} = \frac{E_1}{(1 - \nu_{12}\nu_{21})} \tag{1}$$

$$Q_{22} = \frac{E_2}{(1 - \nu_{12}\nu_{21})} \tag{2}$$

$$Q_{12} = Q_{21} = \frac{\nu_{12}E_2}{(1 - \nu_{12}\nu_{21})} = \frac{\nu_{21}E_1}{(1 - \nu_{12}\nu_{21})} \tag{3}$$

$$Q_{16} = Q_{26} = Q_{61} = Q_{62} = 0 \tag{4}$$

$$Q_{66} = G_{12} \tag{5}$$

6

Using these formulas, the [Q] matrix for this composite becomes

$$Q = \begin{bmatrix} 145.07 & 24.26 & 0 \\ 24.26 & 97.06 & 0 \\ 0 & 0 & 42 \end{bmatrix} GPa \qquad (6)$$

The [$\overline{Q}$] matrix which relates the engineering strains to the stresses referred to arbitrary axes is defined by

$$\overline{Q}_{11} = Q_{11}\cos^4\theta + Q_{22}\sin^4\theta + 2(Q_{12} + 2Q_{66})\sin^2\theta\cos^2\theta \qquad (7)$$

$$\overline{Q}_{22} = Q_{11}\sin^4\theta + Q_{22}\cos^4\theta + 2(Q_{12} + 2Q_{66})\sin^2\theta\cos^2\theta \qquad (8)$$

$$\overline{Q}_{12} = (Q_{11} + Q_{22} - 4Q_{66})\sin^2\theta\cos^2\theta + Q_{12}(\cos^4\theta + \sin^4\theta) \qquad (9)$$

$$\overline{Q}_{66} = (Q_{11} + Q_{22} - 2Q_{12} - 2Q_{66})\sin^2\theta\cos^2\theta + Q_{66}(\sin^4\theta + \cos^4\theta) \qquad (10)$$

$$\overline{Q}_{16} = (Q_{11} - Q_{12} - 2Q_{66})\cos^3\theta\sin\theta - (Q_{22} - Q_{12} - 2Q_{66})\cos\theta\sin^3\theta \qquad (11)$$

$$\overline{Q}_{26} = (Q_{11} - Q_{12} - 2Q_{66})\cos\theta\sin^3\theta - (Q_{22} - Q_{12} - 2Q_{66})\cos^3\theta\sin\theta \qquad (12)$$

The X-Axis in this case is defined to be parallel to the loading direction (and the 0° plies) while the Y-Axis is parallel to the 90° plies. Since there are two fiber orientations in this composite, there will be two separate [$\overline{Q}$] matrices. Substituting 0° and 90° for theta in each of the above equations yields

$$\overline{Q}_{[0]} = \begin{bmatrix} 145.07 & 24.26 & 0 \\ 24.26 & 97.06 & 0 \\ 0 & 0 & 42 \end{bmatrix} GPa \qquad (13)$$

$$\overline{Q}_{[90]} = \begin{bmatrix} 97.06 & 24.26 & 0 \\ 24.26 & 145.07 & 0 \\ 0 & 0 & 42 \end{bmatrix} GPa \qquad (14)$$

The extensional stiffness matrix [A] is defined as the sum of the [$\overline{Q}$] matrices multiplied by the individual ply thickness, or in equation form

7

$$A_{ij} = \sum \overline{Q}_{ij}(h_k - h_{k-1})$$

(15)

The thickness of each ply is the term $(h_k - h_{k-1})$ and is calculated by dividing the total thickness of the plate by the number of plies. Substituting this along with the two $[\overline{Q}]$ matrices yields

$$A_{ij} = \begin{bmatrix} 353.5 & 70.8 & 0 \\ 70.8 & 353.5 & 0 \\ 0 & 0 & 122.6 \end{bmatrix} MPa$$

(16)

With the [A] matrix now known, the following formula which is applicable to a symmetrical lay-up can be used in which N_x, N_y, and N_{xy} are the external forces/unit width and ϵ_x, ϵ_y, and γ_{xy} are the mid-plane strains

$$\begin{bmatrix} N_x \\ N_y \\ N_{xy} \end{bmatrix} = \begin{bmatrix} A_{11} & A_{12} & A_{16} \\ A_{12} & A_{22} & A_{26} \\ A_{16} & A_{26} & A_{66} \end{bmatrix} \begin{bmatrix} \epsilon_x^0 \\ \epsilon_y^0 \\ \gamma_{xy}^0 \end{bmatrix}$$

(17)

Since the loading direction in this study is only in the X-direction, the standard elastic stress-strain formula is applicable

$$E_x = \frac{\sigma_x}{\epsilon_x^0}$$

(18)

By inverting the [A] matrix in Eq (17), setting N_y and N_{xy} to zero, and solving for the strains, the modulus in the loading direction E_x for the laminate can then be predicted by the following formula

$$E_x = \frac{A_{11}A_{22} - A_{12}^2}{tA_{22}} = 116 \ GPa$$

(19)

In a similar manner, if the modulus in the transverse direction were required, this could be predicted by

8

$$E_y = \frac{A_{11}A_{22} - A_{12}^2}{tA_{11}} = 116 \; GPa \qquad (20)$$

From the initial static tension test, using a least squares fit, the measured value of the modulus in the loading direction E_x was 120 GPa, or within four percent of this predicted value.

The Total Ply Discount Method can also be applied. Since the strength of the 90° plies is less than that of the 0° plies, the 90° plies will fail first. When this occurs, only the 0° plies will be sustaining the load. The same $[\bar{Q}]$ matrices can be used except that the $[\bar{Q}]_{90}$ matrix becomes zero since it is fully "discounted." A new [A] matrix is then calculated to be

$$A_{ij} = \begin{bmatrix} 211.8 & 35.4 & 0 \\ 35.4 & 141.7 & 0 \\ 0 & 0 & 61.3 \end{bmatrix} \qquad (21)$$

The modulus E_x in the loading direction becomes 69.5 GPa or sixty percent of the initial modulus. This is reasonable since the measured modulus during tension-tension tests fell to seventy percent after the first cycle and then to a fairly constant final value of fifty percent.

9

III. Experimental Procedure

A. Test Station

     The test stand consisted of five primary items: the test frame, the control console, a personal computer, a Wavetek function generator, and a gripping system. The test frame was an MTS with a 22.2 KN MTS Servoram Actuator. The control console was dominated by the MTS 458.20 Microconsole, but also included an MTS 464.80 Data Display, a Measurements Group 2310 Signal Conditioning Amplifier, and an oscilloscope. The personal computer was an IBM PC AT with a 286 chip whose primary purpose was to house the testing software. The Wavetek was a model 75 Arbitrary Waveform Generator which was able to create various input functions. Air pressure was supplied which fed an Haskel Air-Driven Fluid Pump which in turn provided pressurized air to actuate pistons mounted on the test station grip fixtures. Figure 1 shows the setup.
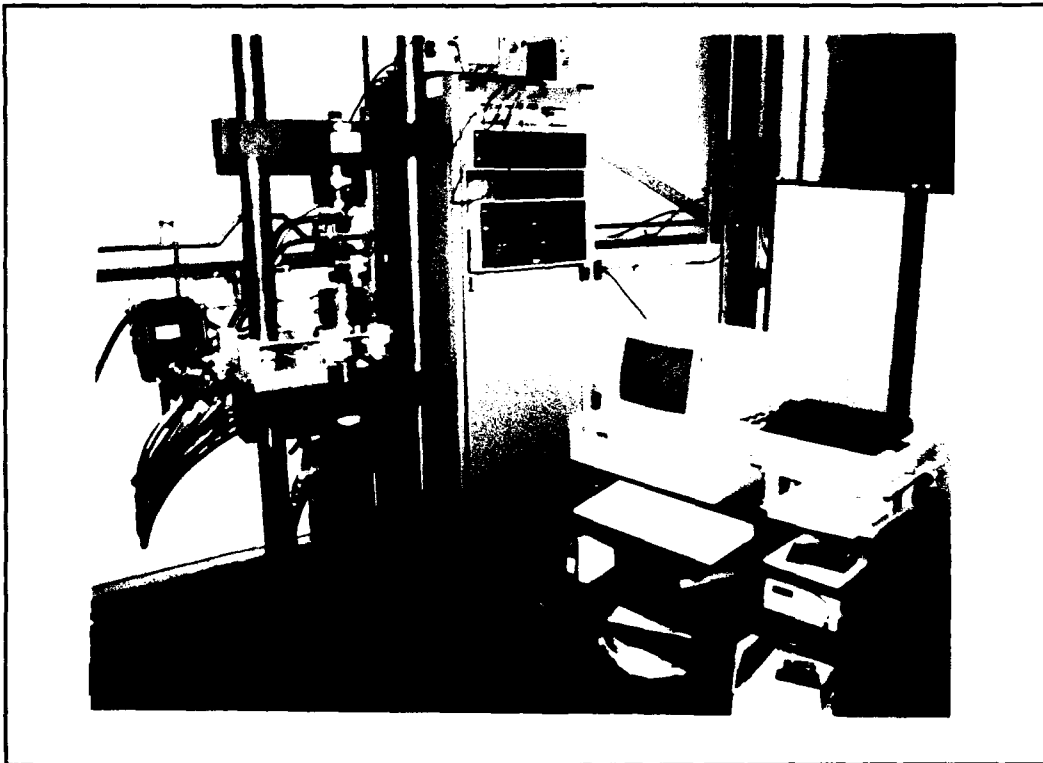

Figure 1
(Test Station)

B. Test Station Alignment

Before any test could be conducted, the test machine had to be aligned. The purpose of the alignment was to ensure that only pure tension or compression loads would be transmitted to the specimen. Any misalignment would create bending and non-symmetrical axial loads and strains and, therefore, unreliable data. These additional loads could adversely affect the overall fatigue limit of the specimen and, ultimately, cause premature failure.

The test station itself was previously aligned by the AFIT personnel prior to the first test conducted. An in-depth explanation of the alignment procedure was given by Tracy [10]. In general terms, the alignment was accomplished through use of a Woods Metal Pot. This device consisted of a cylindrical stainless steel plug within another stainless steel cylinder and the gap between the two cylinders filled with Woods metal. The lower grip of the test station was attached to the inner plug, while the upper grip was secured to the test stand. The metal was melted, thus allowing relatively free movement of the inner plug and lower grip. Angle irons were then butted against the upper grip and lower grip and securely fastened, and the metal allowed to dry. Once the metal dried, the angle irons were removed and alignment attained.

To verify the actual grip alignment, a test was performed in accordance with ASTM Procedure E1012-89. A stainless steel square specimen of length 10 cm and sides of length 6.35 mm was fabricated at the AFIT Model Shop. The sides were polished, then four strain gauges were attached, each centered on a side. Wires were then soldered to the strain gauges and connected to a Measurements Group SB-10 Switch and Balance Unit. This in turn was connected to a BLH Model 1200B Digital Strain Indicator from which actual strain measurements were manually recorded. The specimen was inserted into the test station, the grip hydraulic pressure actuated, and the specimen held securely in place and ready for

11

testing.

The strain in the axial direction, a, is defined as the average of the strains on each face, e_i, or

$$a = \frac{(e_1 + e_2 + e_3 + e_4)}{4} \qquad (22)$$

The bending strain on each face is defined as the difference between the axial strain subtracted from the strain on that face, or

$$b_i = e_i - a \qquad (23)$$

The maximum bending strain is defined as the sum of the absolute magnitudes of the bending strains on opposite faces divided by two, or

$$B = \frac{|b_1 - b_3|}{2} + \frac{|b_2 - b_4|}{2} \qquad (24)$$

The percent bending is calculated by

$$PB = \left(\frac{B}{a}\right) x \ 100 \qquad (25)$$

Loads were applied to the specimen in 100 Newton increments and the strains on each gauge manually recorded. In order not to damage either the specimen or the grip inserts, smooth grip inserts were used instead of ridged ones. In order to better match actual test specimen conditions, the grip pressure used was 2500 psi. While this securely held actual test specimens in place, it prevented the alignment load from going above 1,600 Newtons since the alignment specimen tended to begin slipping from the grips at that load level.

Several alignment tests were run. Once data was accurately recorded, the alignment specimen was removed and replaced in the grips but rotated one quarter of a turn. This insured that any discrepancies in strain gauges, either measuring ability or alignment, would be revealed. It was observed that any position other than totally vertical for the

12

alignment specimen resulted in unequal strains and, consequently, bending; therefore, this showed that great care had to be taken when initially placing any test specimens into the grip fixture. Figure 2 shows the percent bending versus the load. The maximum percent bending levelled off under three percent, thus proving that the test station was adequately aligned.

Test Station Alignment
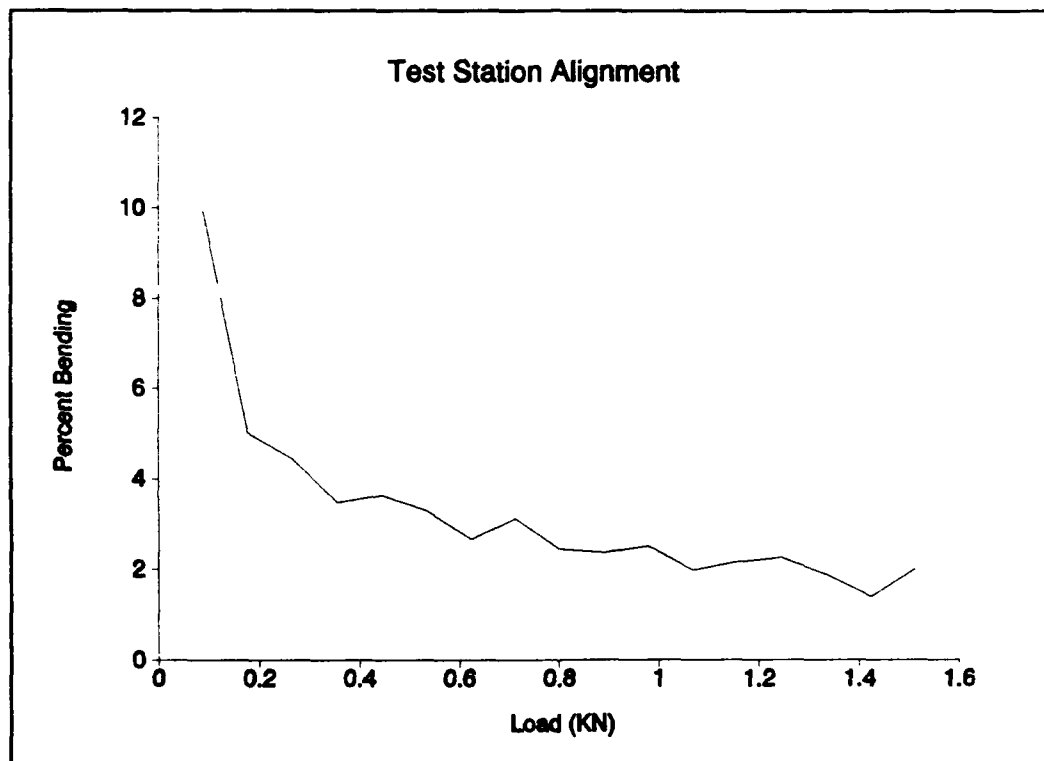
Figure 2
(Test Station Alignment Verification)

C. Specimen Background and Preparation

The material used was a silicon fiber (Nicalon) reinforced calcium-aluminosilicate ceramic matrix composite. Ceramic matrix composites are generally formed by a two-stage process. Agarwal and Broutman [8] state the most common technique first involves passing a fiber tow through a slurry tank (containing the matrix powder, binder, and carrier liquid),

winding it on a drum and then allowing it to dry. Next, the tows are cut and stacked and hot pressed at temperatures above 1200°C to minimize porosity.

Nicalon is an amorphous/crystalline fiber, predominantly silicon carbide, made by the Nippon Carbon Company. It's approximately 15 μm in diameter, and commonly available in an 1800 denier tow. The matrix is a calcium-aluminosilicate crystalline glass-ceramic made by Corning Glass. The composite itself consists of about forty percent fiber by volume.

The Nicalon/CAS composite provided was a 15.25 cm square plate approximately 3 mm thick. Its date of manufacture was 31 October 1990. The plate faces were smooth and covered with a clear protective coating, but the edges were very ragged and loose fibers were clearly visible. In order to maximize the number of tests possible and minimize material waste, each specimen was to be no more than 7.62 cm long and 6.35 mm wide.

The first step was to square the plate and sharpen the edges. All cutting was accomplished using a Buehler Isomet Low Speed Saw. A 0.381 mm thick, 12.7 cm diameter diamond wafering blade at 150 RPM was used to make all cuts. The plate itself was attached to the saw's specimen mounting arm with two C-clamps and was butted up against the diamond wheel. The arm was raised and the blade precisely moved with a micrometer, then the saw started and plate lowered onto the rotating wheel. The plate had to be adjusted in the arm for each cut since the 12.7 cm wheel could not completely cut the 15.25 cm plate at one time.

Twenty-two specimens were eventually cut from the plate. This left a 7.62 cm x 15.24 cm plate available for future use. From these twenty-two specimens, each was measured for uniformity of width and thickness and viewed for any noticeable cracks or damage. The best ones were chosen for actual testing. Figure 3 shows the location of the specimens on the plate.

Once the specimens were cut, they were prepared for testing. The first step involved polishing the edges for any test requiring replicas
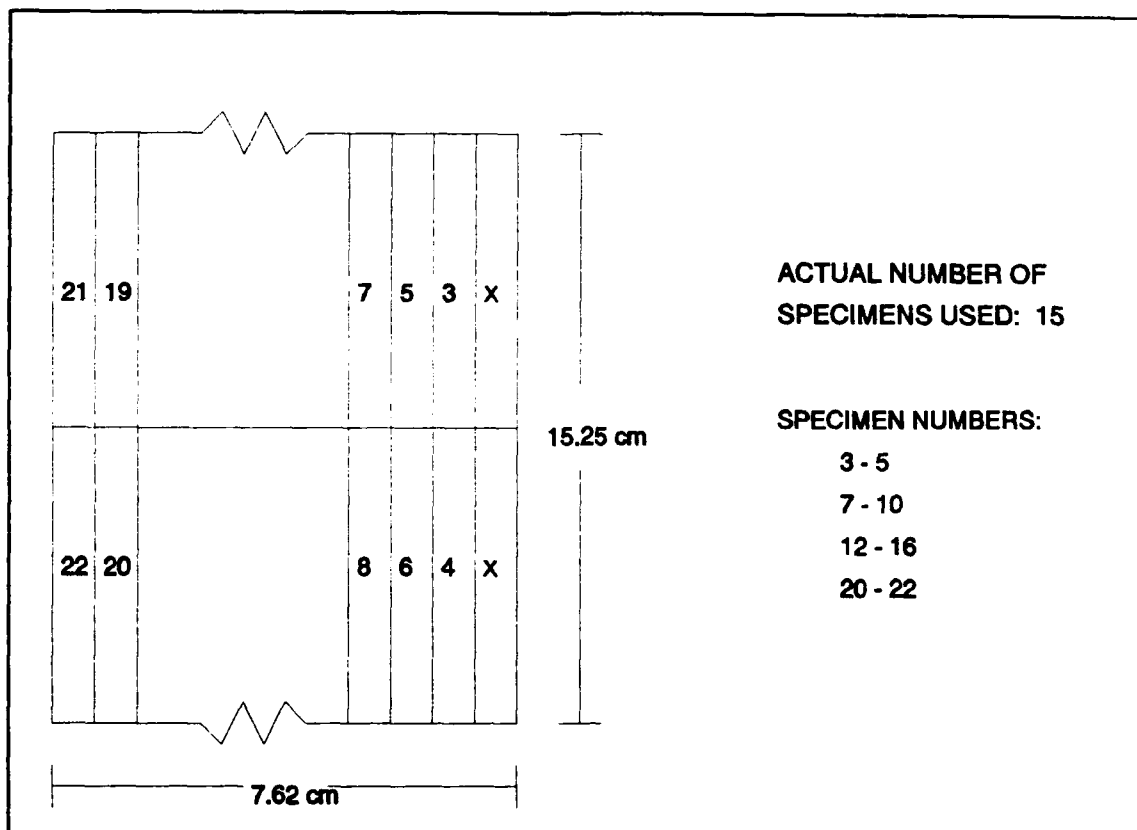
Figure 3
(Test Specimen Locations on Plate)

ACTUAL NUMBER OF
SPECIMENS USED: 15

SPECIMEN NUMBERS:
3 - 5
7 - 10
12 - 16
20 - 22

and/or pictures. This was by far the most time-consuming process. All
polishing was carried out on a 20.3 cm diameter Buehler Polimet I Polisher
at 200 RPM and involved six separate stages. A different type of
polishing disc or cloth was used in each of these stages. A Fine-Grind
Polishing Disc was initially used for twenty minutes which in turn was
followed by thirty minutes of polishing on a Rough-Polish Disc and then by
thirty additional minutes on a Medium-Polish Disc. A nylon cloth was then
attached to the Polimet I wheel and six-micron diamond suspension fluid
sprayed onto the surface. The specimen was then polished for one to two
hours with repeated sprayings of the six-micron fluid. The nylon cloth
was removed, replaced with a new one, and three-micron diamond suspension
fluid was then used. Polishing on this cloth lasted another one to two
hours. Finally, a new nylon cloth was attached and polishing was

15

accomplished for two to three hours using one-micron diamond suspension fluid. After each stage, the specimen was viewed under a microscope to determine if any additional polishing time was required. The final polished specimen clearly showed fibers and matrix in each ply.

The second step in specimen preparation involved attaching fiberglass tabs in order that the the test station grips did not damage or crush the actual test specimen. Each tab was 1.9 cm long, 1.52 mm thick, and cut to the width of the specimen. One end was beveled at thirty degrees. This angle was chosen since a forty-five degree angle used during practice tests tended to break the specimen right in the grip, indicating the angle was not significantly reducing the stress concentration factor. Four tabs were then attached to each specimen using a 50/50 mixture of V-40 Curing Agent and Epoxy Resin and held in place with two two-inch binder clips. The specimen was then placed in an oven at 70° Celsius for ninety minutes and allowed to cure. When removed, the specimen was ready for testing. Figure 4 shows the final configuration of each specimen and its dimensions. Since the program used to run the fatigue tests required the specimen dimensions in English units, the dimensions are shown in English units.

D. Experimental Procedure

Once the specimen's tabs were attached and polishing, if required, was completed, it was ready for testing. The applicable Load Card was first inserted, the size chosen so that it was the minimum necessary to provide the required load. Hydraulic pressure to the test station was actuated via the MTS Microconsole, and the Microconsole was switched to Displacement control so that the grips could be raised and lowered as needed to install the specimen. The air pressure was then turned on and the grip pressure adjusted to approximately 2500 psi.

The specimen was now ready to be installed. The grip inserts were chosen to correspond with any specimen thickness variations so as to

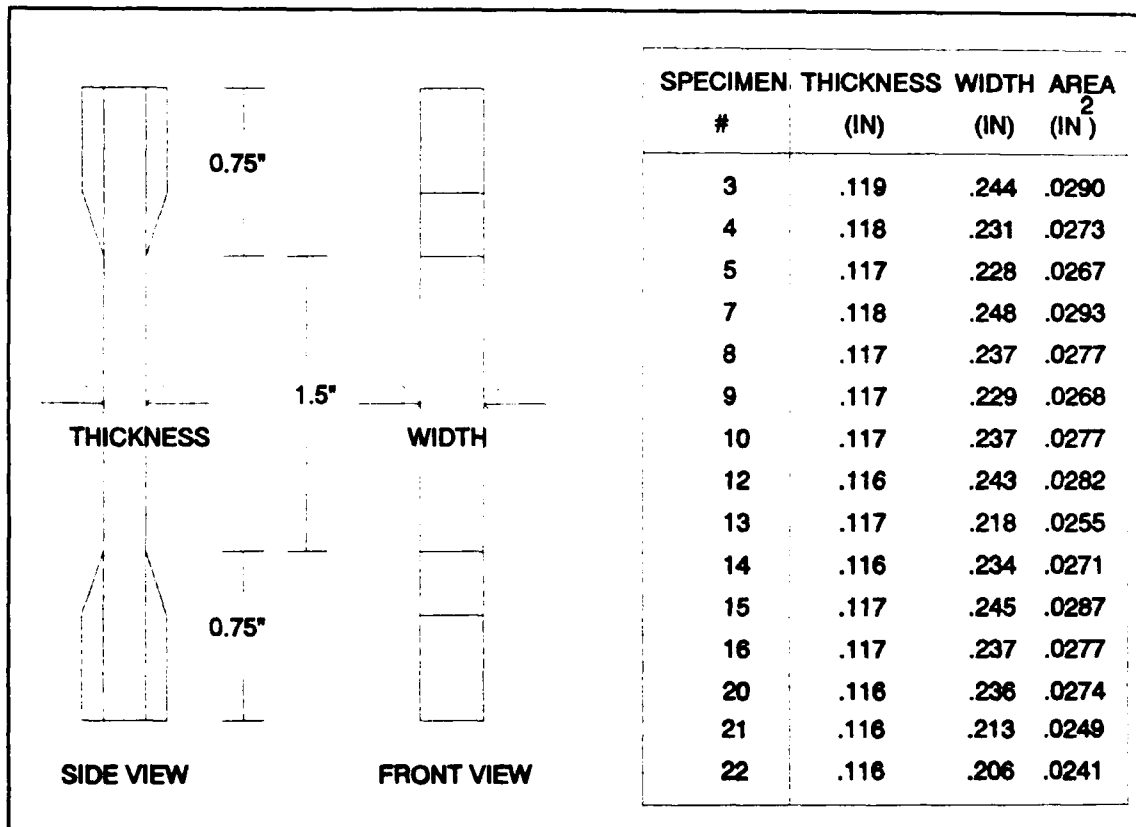| SPECIMEN #	THICKNESS (IN)	WIDTH (IN)	AREA (IN^2)
3	.119	.244	.0290
4	.118	.231	.0273
5	.117	.228	.0267
7	.118	.248	.0293
8	.117	.237	.0277
9	.117	.229	.0268
10	.117	.237	.0277
12	.116	.243	.0282
13	.117	.218	.0255
14	.116	.234	.0271
15	.117	.245	.0287
16	.117	.237	.0277
20	.116	.236	.0274
21	.116	.213	.0249
22	.116	.206	.0241

Figure 4
(Test Specimen Configuration and Dimensions)

provide minimal clearance between the specimen tab and the insert itself. The lower portion of the specimen was placed into the bottom grip, a stainless steel alignment bracket was set onto the top of the bottom grip, and the specimen aligned so as to be flush with the alignment bracket along its length. The grip pressure was then released and the piston actuated, thus forcing the grip closed and securing the specimen in place. The lower grip was then raised so that the upper portion of the specimen was now in the upper grip. The Microconsole was switched back to Load control, and the upper grip pressure released, thus securing the top of the specimen. Alignment was verified again with a depth micrometer. The load was then adjusted so as no load was being placed on the specimen.

The next step involved attaching the clip-on extensometer. Placing the extensometer on the specimen face, a spring was attached to a clip on

17

one side of the extensometer and stretched across the specimen face until it was able to be secured to the clip on the opposite side of the extensometer. A second spring was attached in the same manner. In order to minimize slipping, four additional rubber bands were also used to firmly hold the extensometer in place, two attached to the upper extensometer clips and two to the lower ones. Once attached, the extensometer was zeroed so as to read no strain for no load.

Static tension and compression tests were accomplished and data recorded using a C program called "MODULUS.EXE" written by Capt. Brian Sanders, an AFIT Ph.D. student. The Wavetek was programmed to create a ramping function, and the rate of increasing load was set so as to be 10 MPa per second. The test sequence consisted of running the "MODULUS.EXE" program, and then activating the Wavetek. The increasing load/stress and strain was then stored in an ASCII file for easy retrieval.

Fatigue tests were run using a program called MSNTEST, Version 2.33, MATE Stress/Life Test Control Program, developed by George Hartman of the University of Dayton Research Institute. Tension-tension, tension-compression, and compression-compression tests were all able to be run using this program. A menu systematically asked for various test-unique data, i.e., maximum stress, load ratio, frequency, specimen dimensions. Once this data was entered, the test required no operator inputs and continued until a certain cycle count was reached or specimen failure occurred. All tests were run at 10 Hz using a sine input wave.

Tests which required replicas were able to be put on hold. Replicas were accomplished with the specimen under a tensile load of approximately seventy-five percent of the maximum, thus ensuring that cracks would not be closed and, therefore, visible. The procedure for taking replicas consisted of coating the specimen's edge surface with acetone then quickly placing a piece of acetate over the wetted area and firmly rubbing the acetate to remove any excess fluid or air bubbles. After 45 seconds, the acetate could be removed and, hopefully, an adequate replica was produced.

18

Once the edge replicas were taken, viewed under the microscope and deemed acceptable, they were placed in an oven and baked for thirty minutes at 80° Celsius in order to prevent curling. The best replicas were then chosen from which actual photographs were taken. Figure 5 shows the location and orientation of the photographs that will subsequently be viewed in this thesis as well as the loading direction.
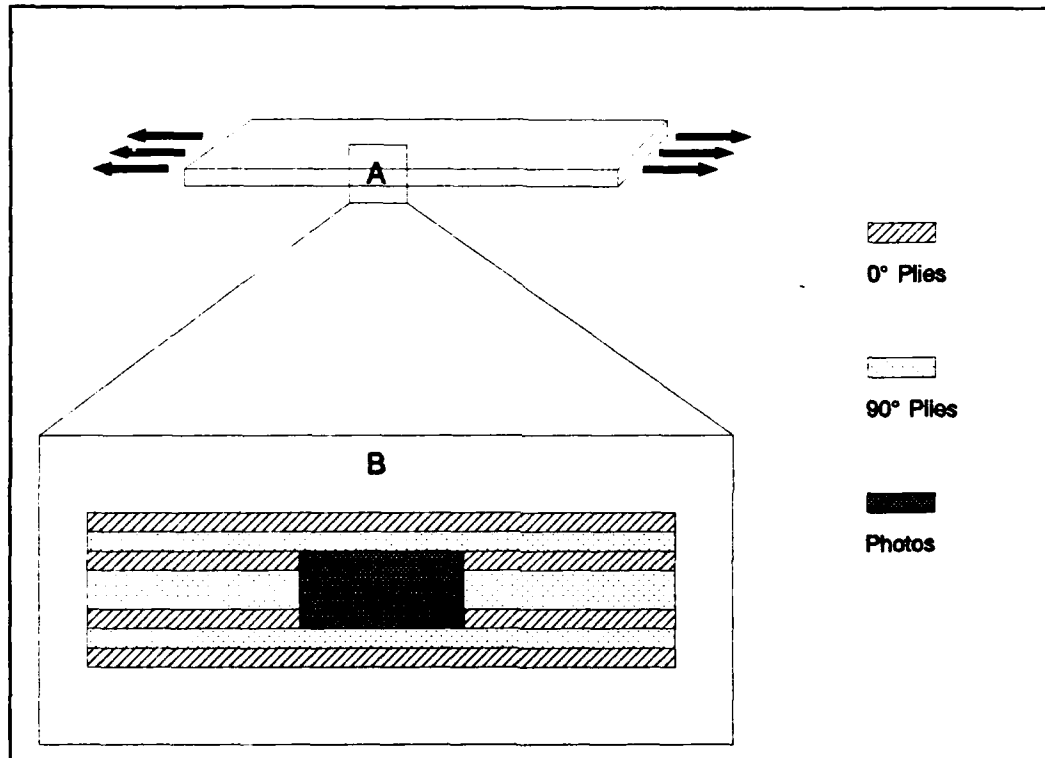

Figure 5
(Edge Replica/Photograph Orientation)

Box A in Figure 5 shows the location on the specimen edge from which replicas were taken. Box B in Figure 5 shows an enlarged view of Box A along with the actual plies. Box C in Figure 5 shows the portion of the replica that was used and shown in each photograph.

IV. Results and Discussion

The primary purpose of this study was to investigate the room-temperature fatigue response of Nicalon/CAS under tension-compression loading. In order to fully understand the failure mechanisms involved in this type of loading, other types of responses had to be identified first: the static behavior in both tension and compression and the fatigue response under tension-tension and compression-compression. Section A will cover the types of tests conducted and their outcomes while Section B will analyze these results.

In evaluating specimen damage, plots of the normalized modulus versus cycle count are used as one means of identifying damage. The normalized modulus is the modulus at any cycle divided by the initial modulus, or E/E_i.

A. Results

Table 2 shows the summary of tests accomplished. R is the ratio of the minimum stress divided by the maximum stress $(\sigma_{min}/\sigma_{max})$. σ_{min} is the smallest positive stress for tension-tension tests or the largest negative stress (absolute value of the magnitude) for tension-compression and compression-compression tests. σ_{max} is the largest postive stress for tension-tension tests or the smallest negative stress (absolute value of the magnitude) for tension-compression and compression-compression tests.

Before any fatigue test was begun, how the composite behaved under static loading was needed; therefore, two static tension tests and one static compression test were conducted. Figure 6 shows the stress-strain curve for the static tension test

In tension, cracking occurred in various stages. Transverse cracks initially developed in the middle 90° plies by 50 MPa, then they began forming in the outer 90° plies. Transverse crack density gradually increased by 100 MPa and transverse cracks began forming in the 0° plies. By 125 MPa, cracks had formed along the entire width of the specimen. At

20

TABLE 2

SPECIMEN #	TYPE OF TEST	MAXIMUM STRESS (MPa)	R	CYCLES
3	STATIC TENSION	275	---	---
21	STATIC TENSION	273	---	---
4	STATIC COMPRESSION	504	---	---
10	TENSION-TENSION	180	0.1	1,609
7	TENSION-TENSION	160	0.1	50,443
9	TENSION-TENSION	140	0.1	1,000,000*
22	TENSION-TENSION	140	0.1	1,000,000*
12	COMPRESSION-COMPRESSION	-140	10.0	1,000,000*
5	TENSION-COMPRESSION	140	-1.0	1,000,000*
14	TENSION-COMPRESSION	140	-1.0	1,000,000*
15	TENSION-COMPRESSION	140	-2.0	10,816
13	COMPRESSION-COMPRESSION	-210	10.0	1,000,000*
8	TENSION-COMPRESSION	140	-1.5	377,176
16	TENSION-COMPRESSION	140	-1.5	250,010
20	TENSION-COMPRESSION	140	-1.5	350,330
	* indicates test was stopped and specimen did not fail			

150 MPa, the existing transverse cracks began bifurcating into additional cracks from the initial ones. By 175 MPa, these new cracks spanned the entire width of the specimen, extending through the 0° and 90° plies, and their density in the 0° plies increased through 250 MPa. At this point, the 0° fibers began breaking, thus leading to ultimate failure by 275 MPa.

A second static tension test was conducted to verify the results of the first and determine if placing the test on hold in order to take acetate-replicas affected the results. The ultimate strength was found to be 273 MPa with an initial elastic modulus of 119 GPa. This data was within two percent of the first test for both the ultimate strength as well as the modulus. Figures 7 through 11 show the sequence of crack progression for the static tension test.
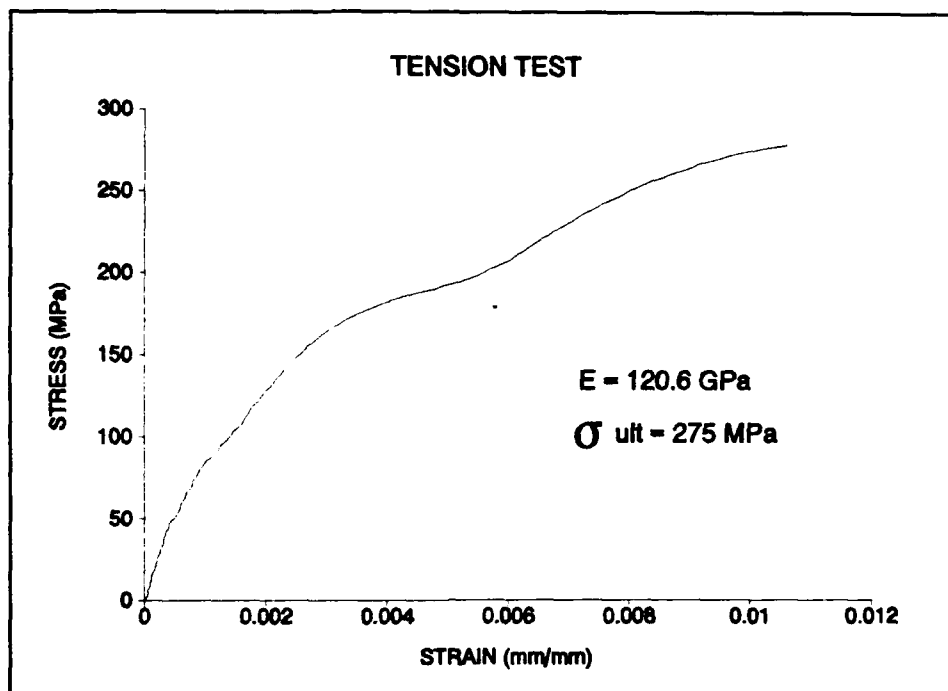
21

TENSION TEST

E = 120.6 GPa

σ ult = 275 MPa

STRESS (MPa)

STRAIN (mm/mm)

Figure 6
(Static Tension Test)

Figure 7
(Static Tension Test, 75 MPa, 50X)

22

Figure 8
(Static Tension Test, 125 MPa, 50X)

Figure 9
(Static Tension Test, 175 MPa, 50X)

Figure 10
(Static Tension Test, 250 MPa, 50X)

Figure 11
(Static Tension Test, 250 MPa, 100X)

Once the static tension test was completed, a static compression test was run. The stress-strain curve was linear up to failure, as shown in Figure 12, and no signs of cracking were noticed with replicas taken through 400 MPa. The specimen failed at 504 MPa. The Euler buckling equation for a column fixed at both ends was used ($P = 4\pi^2 EI/L^2$) with the load at which failure occurred less than the load required for buckling.
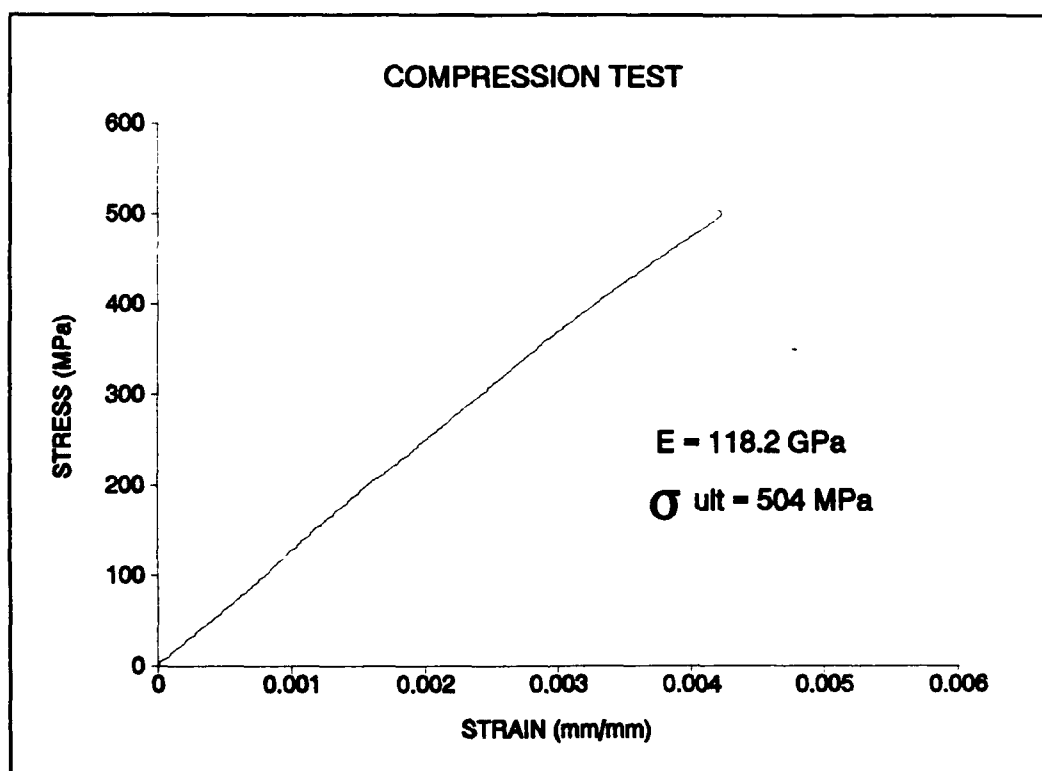
Figure 12
(Static Compression Test)

Now that the static tensile and compressive behavior of the composite was known, the next series of tests involved identifying the threshold for which cycle runout (1,000,000 cycles) would occur under tension-tension fatigue loading. Based on the static tension test curve, tests were conducted at maximum stresses of 180 and 160 MPa, these just above the second "bend" in the curve, both of which failed at 1,609 and 50,443 cycles, respectively. Figures 39 and 40 in the Appendix show the stress-strain curves and the normalized modulus for the 180 MPa test, while Figures 41 and 42, also in the Appendix, show the same curves for

the 160 MPa test. The next test was performed at a maximum stress of 140 MPa, and cycle runout was reached. Figure 13 shows the stress-strain curves while Figure 14 shows the normalized modulus versus cycles.
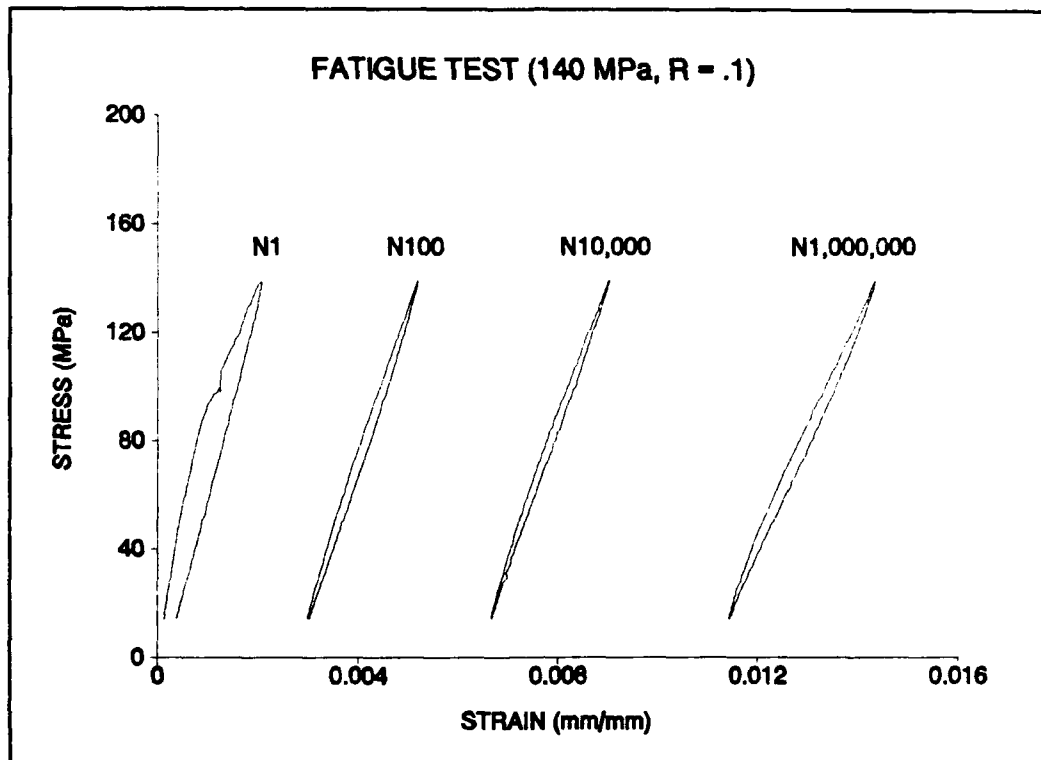

Figure 13
(140 MPa Tension-Tension Test, R = 0.1)

A second fatigue test at a maximum stress of 140 MPa and R = 0.1 was then conducted. Its purpose was to verify the behavior of the initial test as well as provide replicas in which crack growth could be recorded. This test also achieved cycle runout. Most damage occurred during the initial cycle, with transverse cracks running the entire width of the specimen in the 0° and 90° plies. As the number of cycles increased, the transverse crack density increased somewhat with some crack bifurcation until approximately 10,000 cycles, after which the cracks remained relatively constant up to runout. Figures 15 through 17 show the crack progression with very little difference between the last cycle and first.
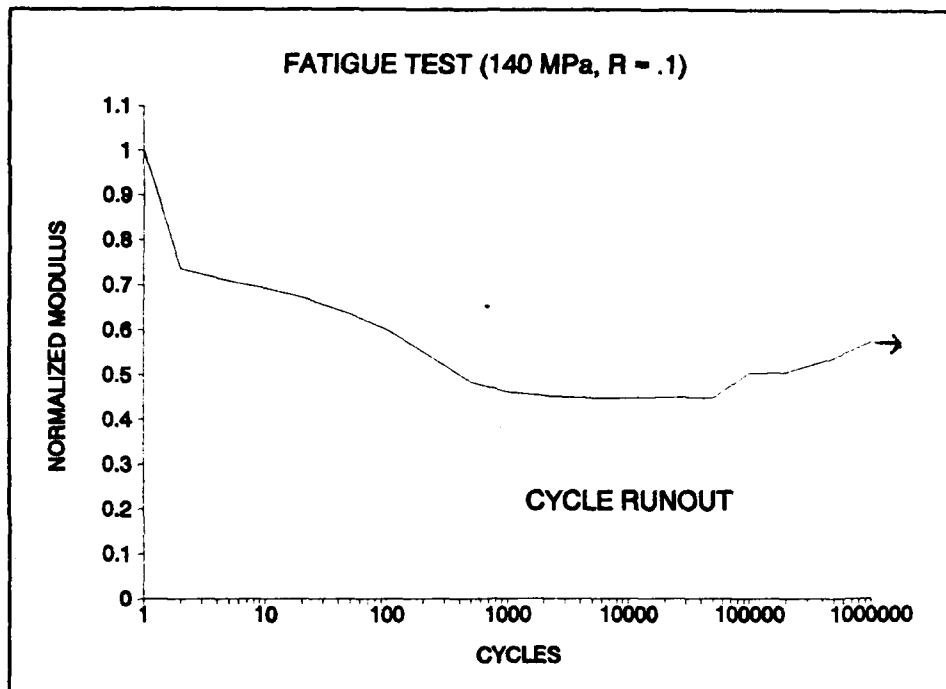
26

Figure 14
(140 MPa Tension-Tension Test, R = 0.1,
Normalized Modulus vs Cycles)

Figure 15
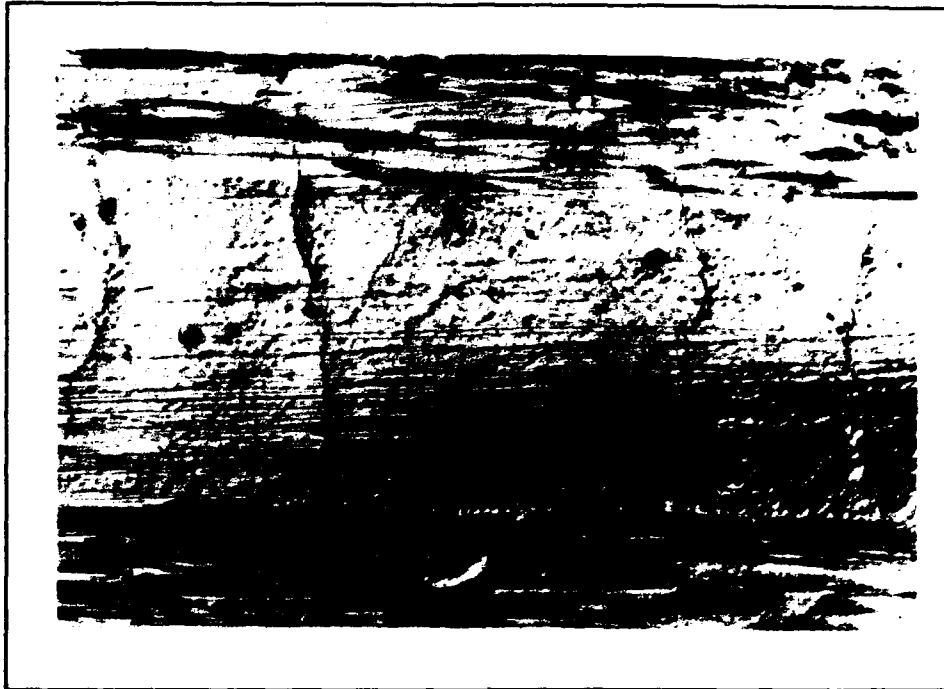(140 MPa Tension-Tension Test, R = 0.1, Cycle 1, 50X)

27

Figure 16
(140 MPa Tension-Tension Test, R = .1, Cycle 10,000, 50X)

Figure 17
(140 MPa Tension-Tension Test, R = .1, Cycle 1,000,000, 50X)

28

The maximum stress for which 1,000,000 cycles would be reached in a tension-tension environment for Nicalon/CAS was, therefore, determined to be 140 MPa. The next step in this study was to examine the effects, if any, that tensile-compressive loads would produce in this composite; however, a compression-compression test had to be run to verify that the compression portion by itself did not inflict any damage. The first load ratio chosen was 10.0 with a maximum compressive stress of 140 MPa, and cycle runout was reached. Figures 18 and 19 show the stress-strain curves and normalized modulus with respect to cycles for this compression test, respectively. The loading and unloading curves for each cycle were nearly identical. The modulus remained within 95% of its initial value after 1,000,000 cycles, and replicas showed no cracks at any time, all of which indicated that the compression-compression cycles caused no damage.
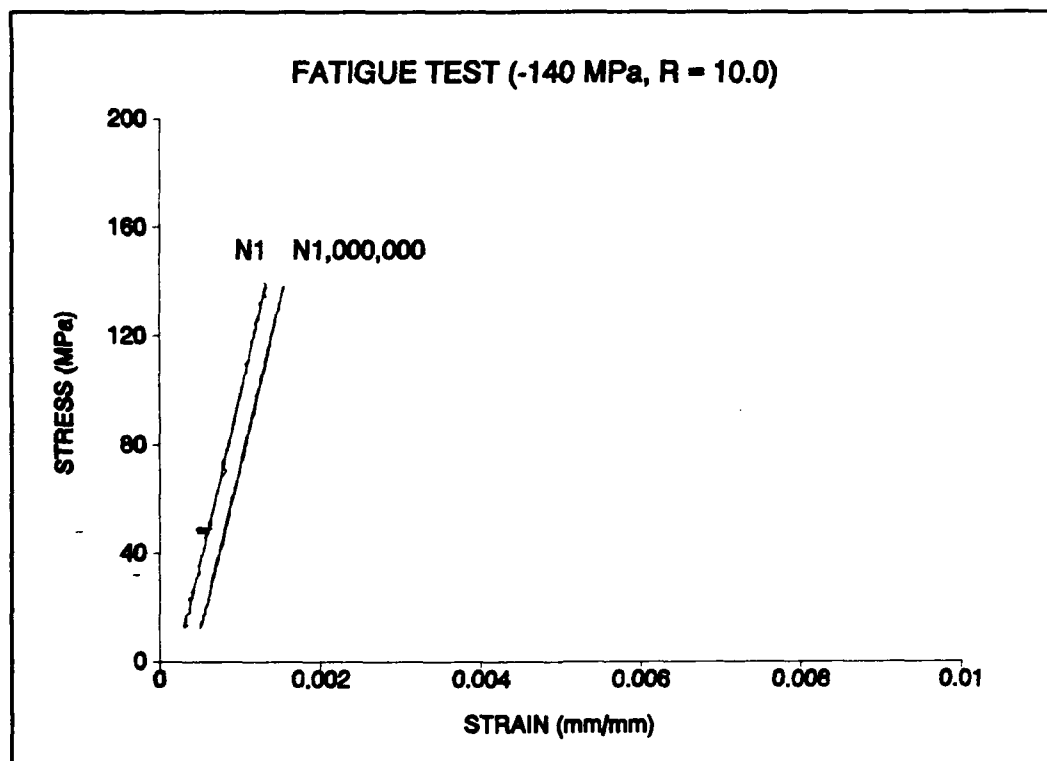
FATIGUE TEST (-140 MPa, R = 10.0)

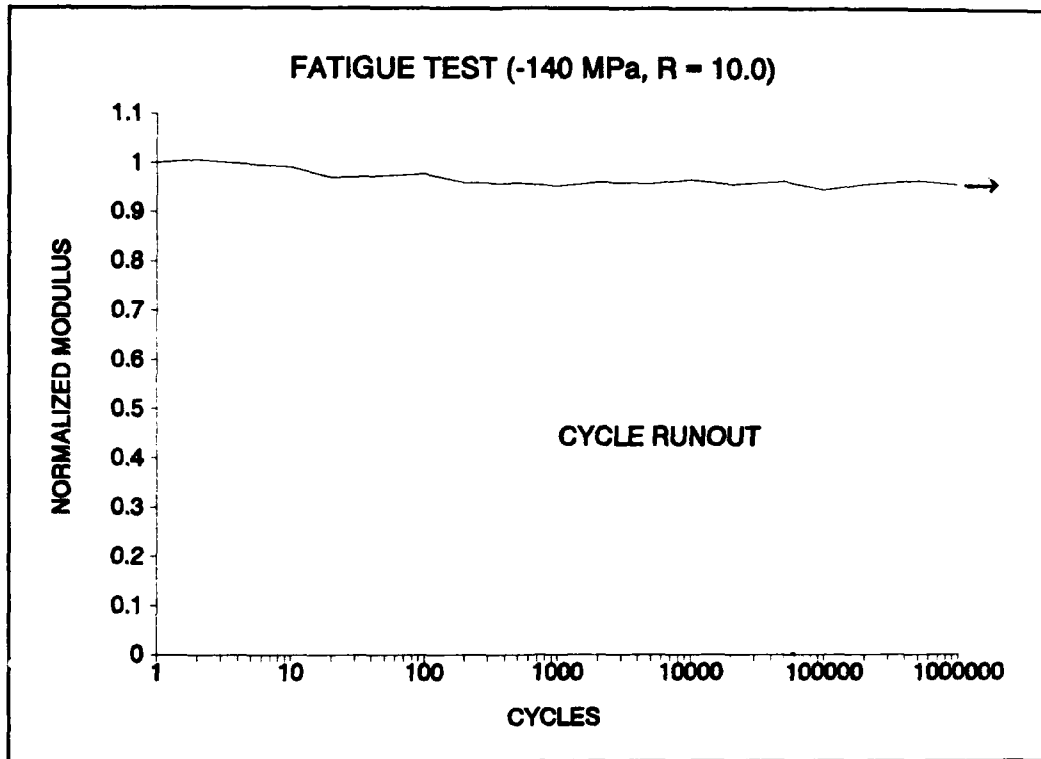Figure 18
(140 MPa Compression-Compression Test, R = 10.0)

Figure 19
(140 MPa Compression-Compression Test, R = 10.0,
Normalized Modulus vs Cycles)

The first full tension-compression test was now ready to begin. A load ratio of -1.0 was chosen, i.e., cycling the specimen back and forth between equal and opposite stresses. Figure 20 shows the stress-strain curve for the test, while Figure 21 shows the normalized modulus with respect to cycles. This test achieved cycle runout.

A second test was then run with replicas. Just like in the tension-tension tests, significant damage occurred during the first cycle with the development of transverse cracks spanning the entire width of the specimen. By 50,000 cycles, these cracks had started bifurcating with the crack density increasing. At approximately 450,000 cycles, however, longitudinal cracks formed in the middle 90° plies. Within the next few hundred thousand cycles, these longitudinal cracks began interacting with the transverse ones, causing an increase in the transverse cracks and
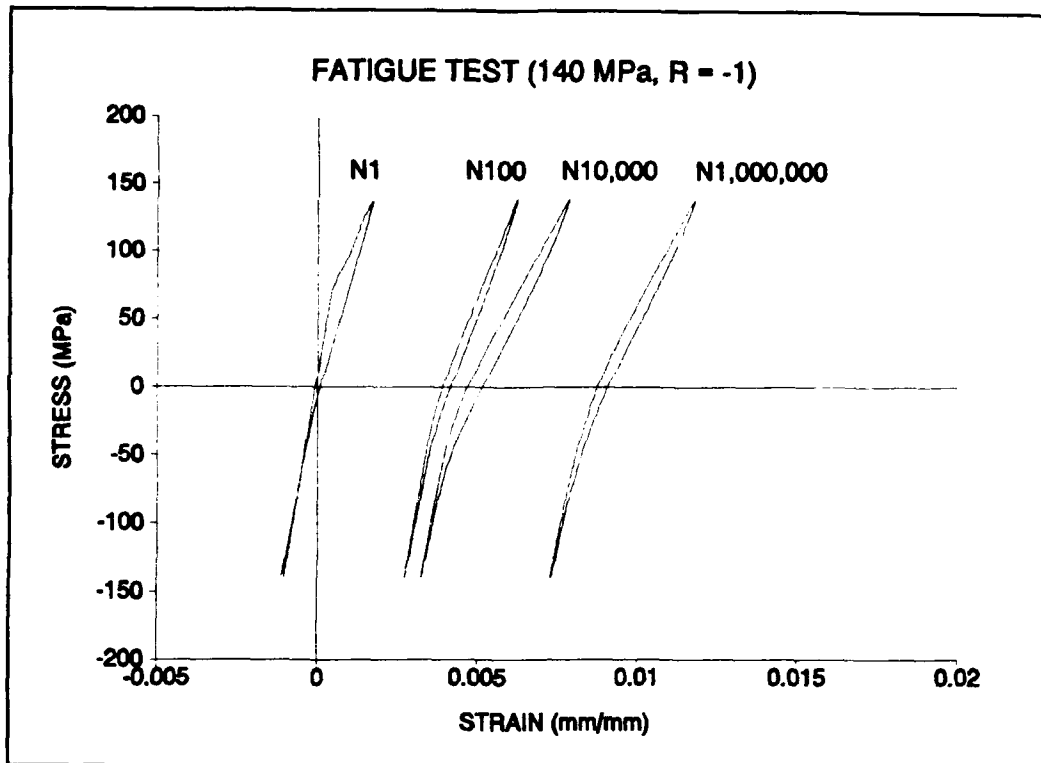
30

Figure 20
(140 MPa Tension-Compression Test, R = -1.0)

lengthening the longitudinal ones. By 1,000,000 cycles, additional longitudinal cracks had formed in the middle and outer 90° plies and ran the entire length of the specimen. This crack development is shown in Figures 22 through 25. While it should be noted that cycle runout did occur, it's clearly evident that significant damage had been sustained. Had 1,000,000 cycles not been chosen as a stopping point, in all likelihood, the damage shown at 1,000,0000 cycles appeared to have been progressing and failure could have occurred had the test been allowed to continue.
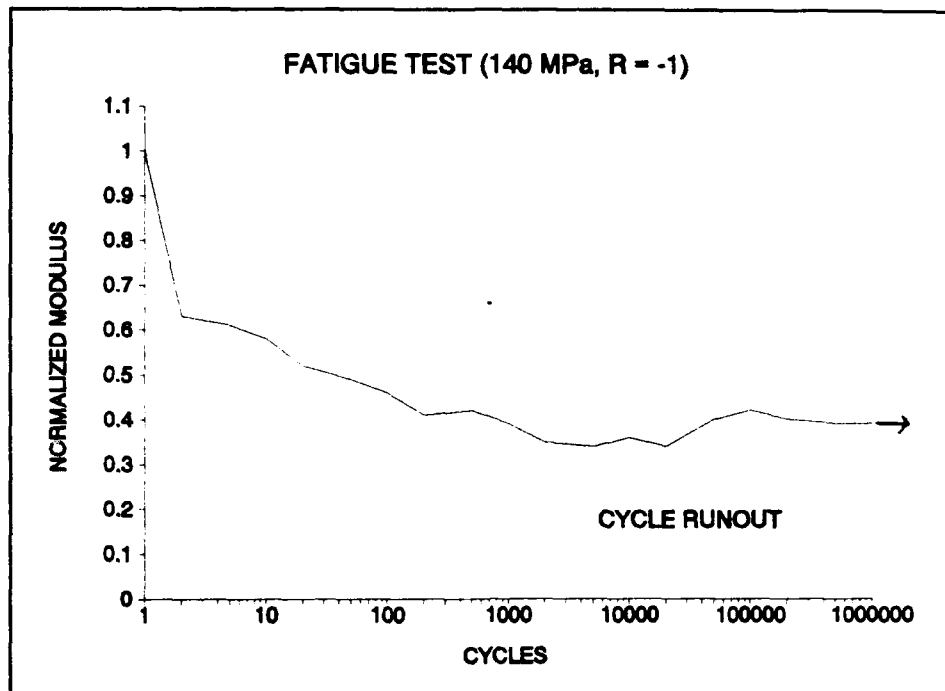
Figure 21
(140 MPa Tension-Compression Test, R = -1.0,
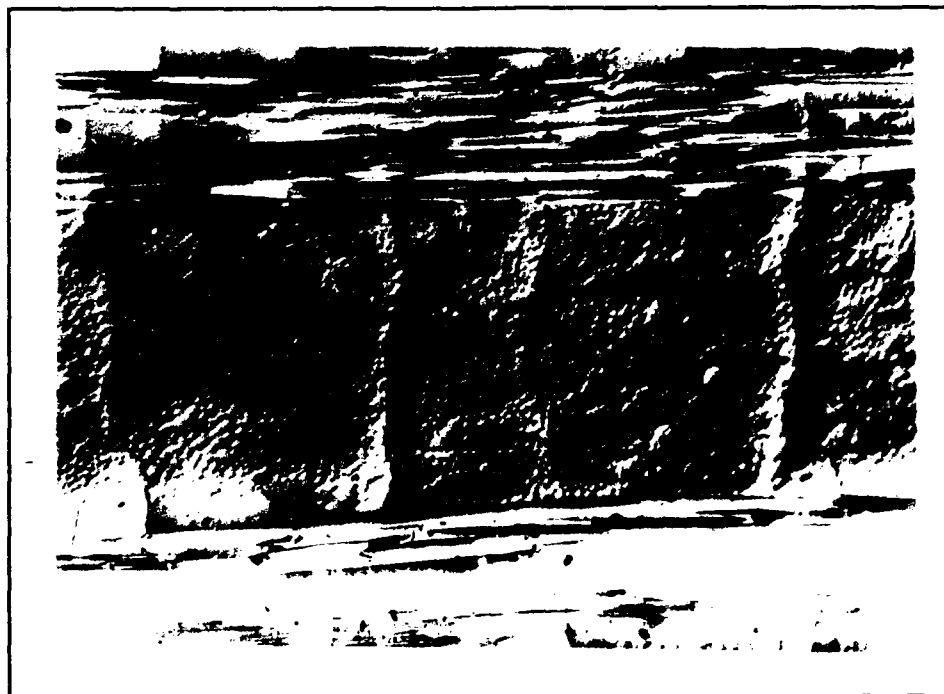Normalized Modulus vs Cycles)

Figure 22
(140 MPa Tension-Compression Test, R = -1.0, Cycle 1, 50X)

32

Figure 23
(140 MPa Tension-Compression Test, R = -1.0,
Cycle 50,000, 50X)

Figure 24
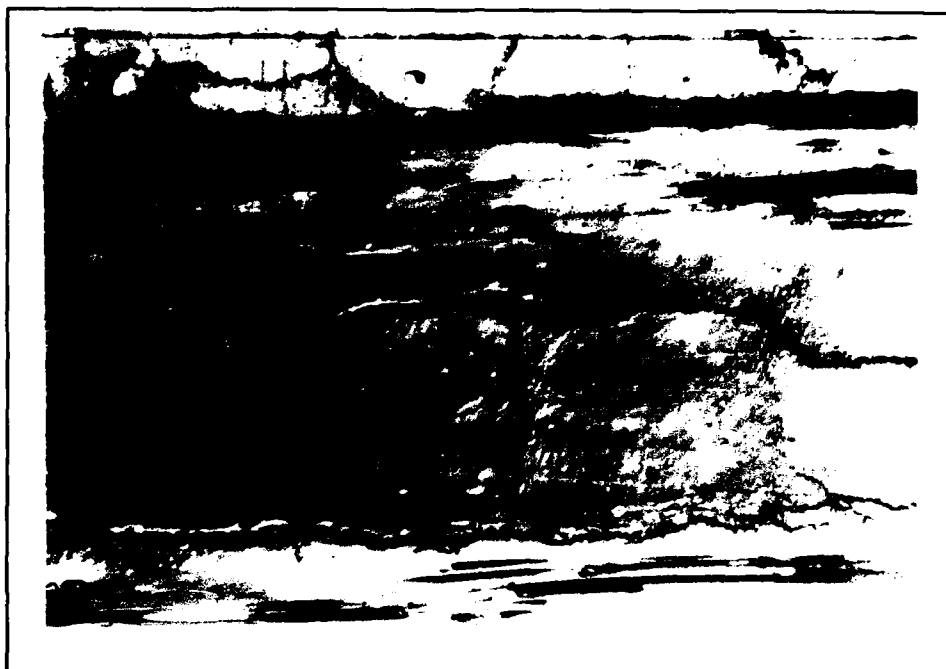(140 MPa Tension-Compression Test, R = -1.0,
Cycle 700,000, 50X)

33

Figure 25
(140 MPa Tension-Compression Test, R = -1.0,
Cycle 1,000,000, 50X)

Now having completed the first series of tension-compression tests at a load ratio of -1.0, the next step was to determine how an increased compressive load would affect the composite. A tension-compression test was performed at a load ratio of -2.0 with a maximum tensile stress of 140 MPa and a maximum compressive stress of 280 MPa. This specimen failed after 10,816 cycles. The failure occurred in compression and clearly showed delamination. Figures 43 and 44 in the Appendix show the stress-strain curves and normalized modulus versus cycles, respectively.

The composite now having survived 1,000,000 cycles at a load ratio of -1.0 and having failed at a load ratio of -2.0, the next logical step was to study the effects at a load ratio of -1.5. Again, in order to assure that the compressive portion by itself was not causing the damage, another compression-compression test was run at a maximum compressive stress of 210 MPa. Figure 45 in the Appendix shows the stress-strain curves while Figure 46 shows the normalized modulus versus cycles. Just

like in the previous compression-compression test, the loading and unloading portions were nearly identical, and the modulus after 1,000,000 cycles was within 95% of its original value, thus indicating that no damage had occurred.

Three tension-compression tests at a load ratio of -1.5 were then run. All three failed in compression. Figure 26 shows the stress-strain curve for the second test while Figure 27 shows its normalized modulus versus cycles. The third test was then run with replicas taken. Cracks developed in the same manner as in the tension-compression test at a load ratio of -1.0, but the time at which they occurred was much sooner. Transverse cracks developed within the first cycle, then crack bifurcation started by 10,000 cycles. Longitudinal cracks formed around 175,000 cycles, followed by crack interaction, crack lengthening, and then failure at 350,330 cycles. Figures 28 through 31 show the crack development.
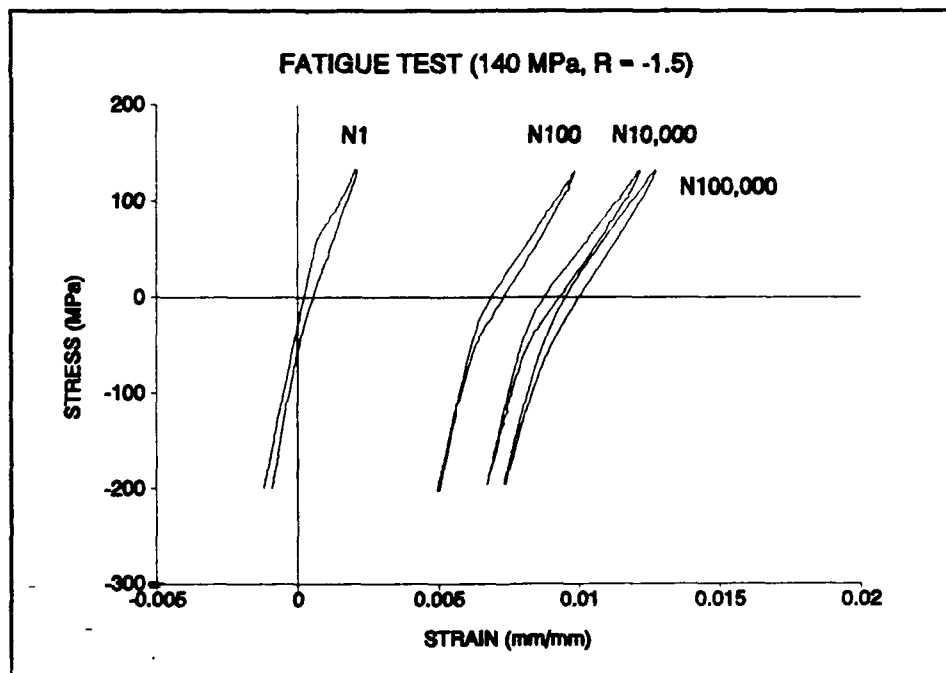

Figure 26
(140 MPa Tension-Compression Test, R = -1.5)

FATIGUE TEST (140 MPa, R = -1.5)
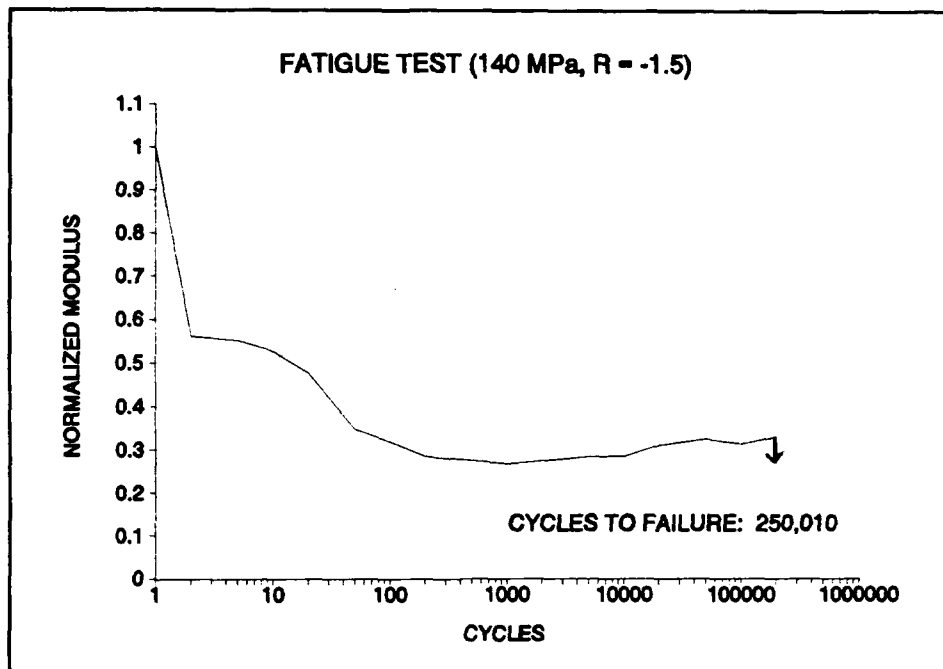
CYCLES TO FAILURE: 250,010

Figure 27
(140 MPa Tension-Compression Test, R = -1.5
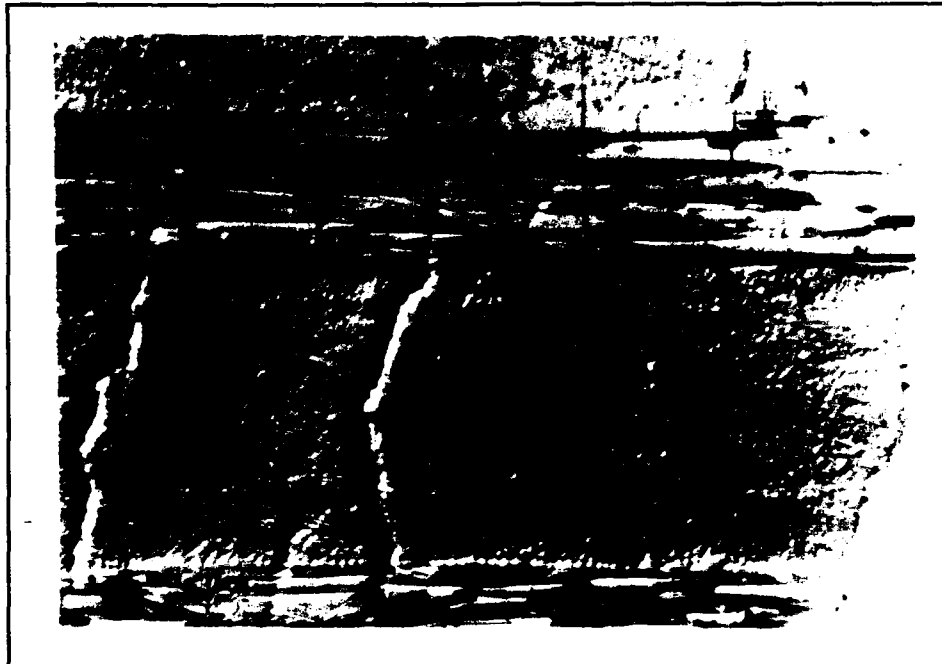Normalized Modulus vs Cycles)

Figure 28
(140 MPa Tension-Compression Test, R = -1.5,
Cycle 1, 50X)

36

Figure 29
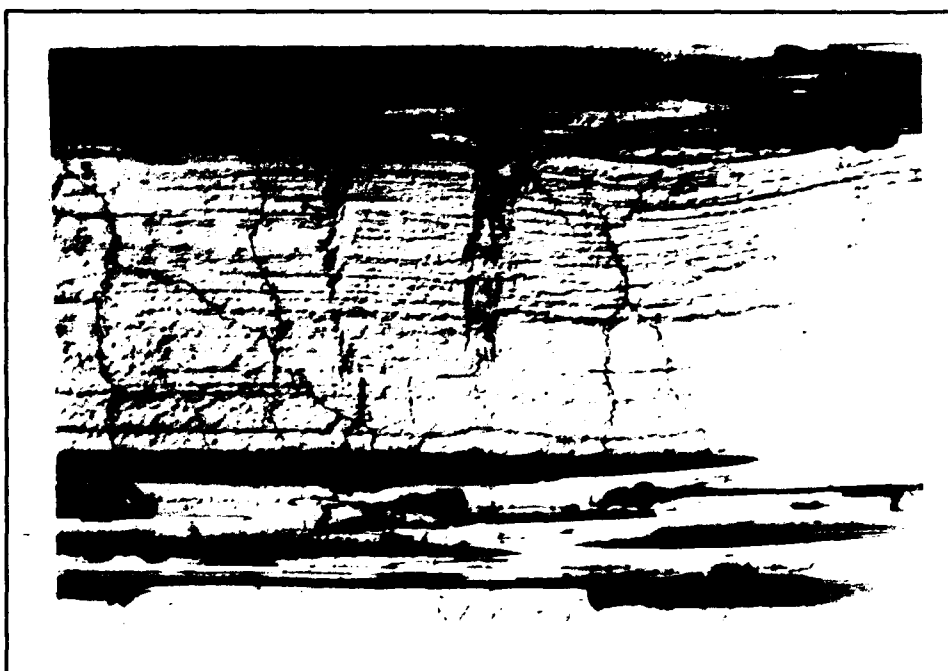(140 MPa Tension-Compression Test, R = -1.5,
Cycle 10,000, 50X)

Figure 30
(140 MPa Tension-Compression Test, R = -1.5,
Cycle 250,000, 50X)

Figure 31
(140 MPa Tension-Compression Test, R = -1.5,
Cycle 350,000, 50X)

B. Discussion

Figure 32 shows a summary of the elastic modulus degradation for the 180, 160, and 140 MPa tension-tension tests. Each modulus dropped to less than seventy percent after the first cycle and then gradually stabilized to approximately fifty percent of its original value by 1,000 cycles. This modulus reduction corresponds to failure of the 90° plies and transfer of the load to the 0° plies and their fibers. As a reminder, the 180 MPa test failed after 1,609 cycles, the 160 MPa test after 50,443 cycles, and the 140 MPa test did not fail and achieved 1,000,000 cycles. What this clearly indicates is that the primary damage, the failure of the 90° plies, occurred almost instantaneously once the test had begun.
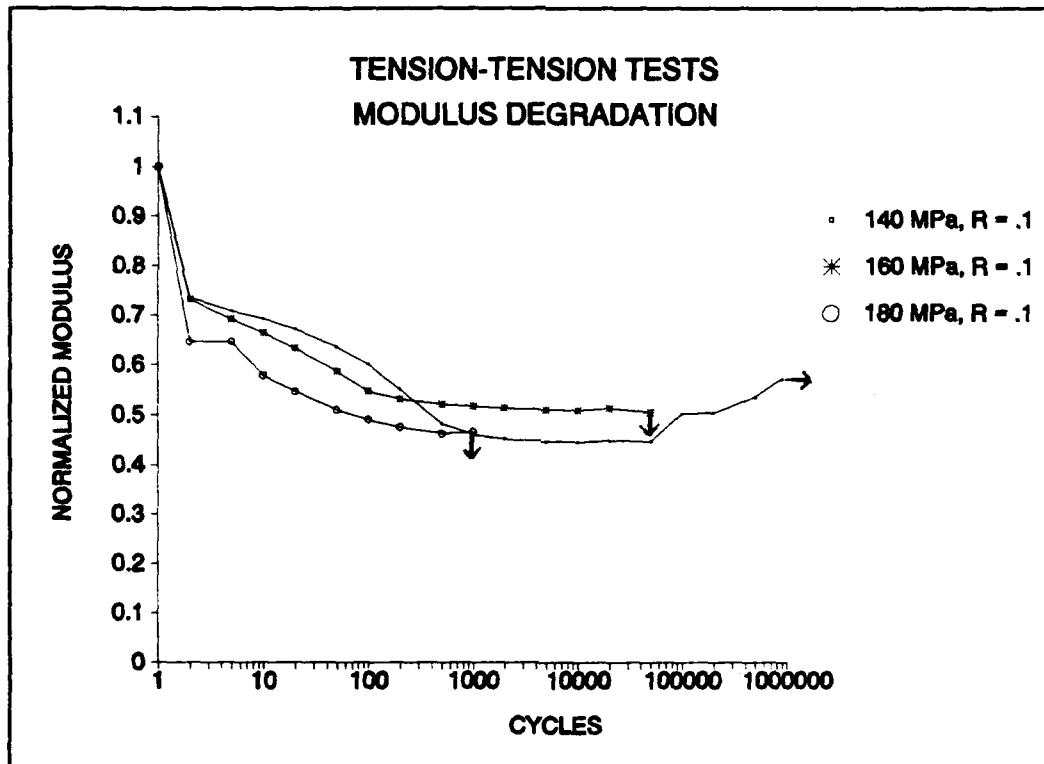

Figure 32
(Tension-Tension Tests, Modulus Degradation)

Since the degradation of the modulus occurred in a similar fashion in each test and in comparable magnitudes, the reason for two to fail and not the third must be explained. Figures 7 through 11 show the crack

39

progression in a static tension test. At 50 MPa, 90° matrix cracking has begun. Since all three tension-tension tests surpassed this value, this cracking obviously occurred in all three specimens. However, the difference between the damage in each becomes more evident at 150 MPa. Above this value, those transverse cracks begin bifurcating and severely increasing in the 0° plies. According to Zawada [15], even with transverse cracks, the matrix in both the 0° and 90° plies still supports a portion of the load. At some point, however, a stress re-distribution occurs in which the matrix becomes unable to support any additional load and the entire stress is transferred to the fibers. Since the load is now distributed over a "smaller" area, the stress is theoretically increased and fiber breakage ultimately occurs. The 150 MPa value is the limit in which the matrix can support a load below that value but eventually fails above it. It is for this reason that tension-tension tests at 160 and 180 MPa failed but the test at 140 MPa achieved cycle runout. Figure 33 shows the fracture surface of the 160 MPa tension-tension specimen.
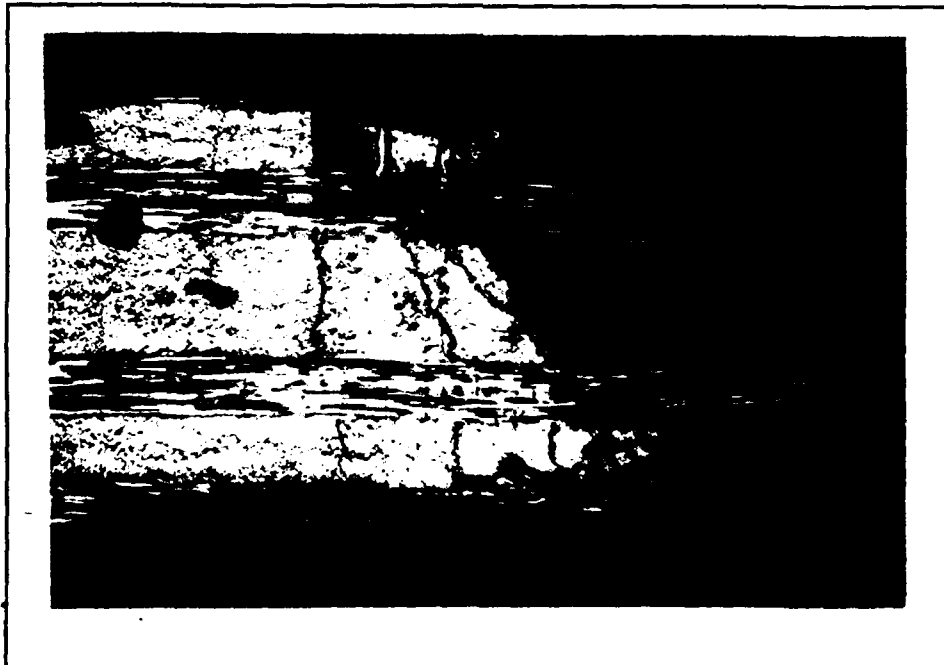

Figure 33
(160 MPa Tension-Tension Test,
R = 0.1, Fracture Surface)

The transverse cracks in the 90° plies are clearly visible, and the number of smaller transverse cracks in the 0° plies is fairly high. Failure occurred with total failure of the 90° plies along with matrix failure in the 0° plies and delamination between the two types of plies.

With the failure mechanism of the tension-tension tests now reasonably known, the next emphasis will be on the tension-compression tests. As a reminder, compression-compression tests were conducted, and these produced minimal, if any, damage to the specimen by themselves. Three types of tension-compression tests were then run with a maximum stress of 140 MPa and load ratios of -1.0, -1.5, and -2.0. As a refresher, these tests achieved cycle runout, failed after 250,020 cycles, and failed after 10,816 cycles, respectively. Figure 34 shows the elastic modulus degradation for these tests.
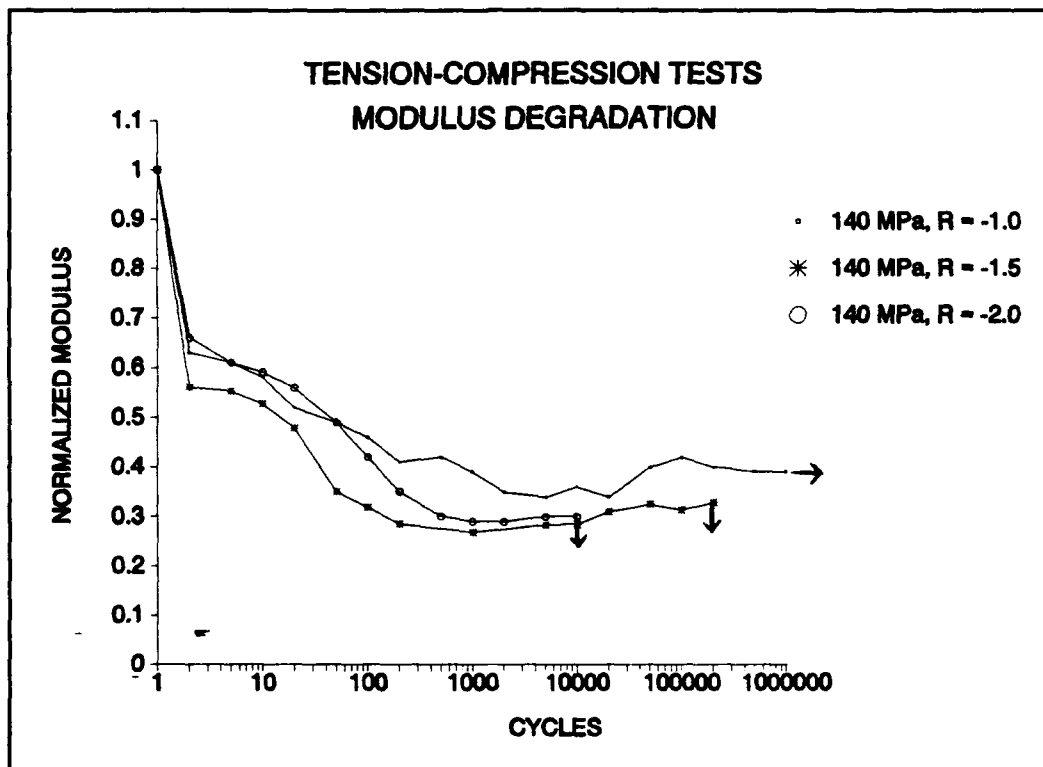

Figure 34
(Tension-Compression Tests, Modulus Degradation)

41

This is very similar to the tension-tension modulus degradation curves. Here, each modulus also dropped to about sixty percent of its initial value after the first cycle and then gradually stabilized after 1,000 cycles to approximately thirty percent of its initial value, somewhat less than the fifty percent value in the tension-tension tests. And just like in the tension-tension tests, two of the three specimens failed before reaching 1,000,000 cycles. The significant reduction in the modulus during the first few cycles again confirms the failure of the 90° plies. One noticeable difference between the failure of the tension-tension specimens from the tension-compression ones is that all tension-compression specimens which did fail did so in compression. Figure 35 shows the fracture surface of a failed specimen in an R = -1.5 tension-compression test. The difference between the two types of failure modes can be attributed to the development of the longitudinal cracks in the tension-compression specimens. Eventually, these cracks become large enough so that the specimen can no longer support compressive loads even though the 0° fibers are intact and buckling of individual plies results.

Looking at the stress-strain curve for the 140 MPa tension-compression fatigue test in Figure 20, one notices that the apparent point at which the loading and unloading curves contact each other occurs at a higher compressive stress as the number of cycles increases. Talreja [14] had shown that slipping and/or sliding occurs as the crack front advances and, as the load is reversed, the surfaces recede unequally because of differences in the stress states on each side of the crack. This mismatch results in a non-linear portion during unloading.

One observation about the plots of the normalized modulus versus cycle count is that, in several instances, the normalized modulus is actually increasing even after several hundred thousand cycles. This phenomenon has been seen in several studies with Zawada [4] theorizing that debris from previous damage may be filling in the voids and preventing full closure of cracks upon unloading. Also, fibers which have

Figure 35
(140 MPa Tension-Compression Test,
R = -1.5, Fracture Surface)

previously debonded may be realigning themselves into a stiffer orientation as the specimen continues to cycle.

The use of a normalized modulus to measure damage is a legitimate approach but not necessarily an entirely accurate one. In each of the tests conducted so far, the modulus substantially decreased within the first few cycles and then eventually levelled off after a few thousand. Once this levelling off occurred, the ability to predict when that specimen would fail was simply not possible. Figure 36 shows a summary of the normalized modulus vs cycles for each test conducted. Another approach to predicting failure was required. One such method used was an energy calculation one.

In using an energy approach, the stress strain curves for various cycles are recorded and the area under each curve is calculated. For a stress-strain curve with MPa (MN/m^2) as the ordinate and strain (m/m) as the abscissa, the units for area become $MN-m/m^3$, or MJ/m^3. This is an energy per unit volume value and can be used to compare data for specimens
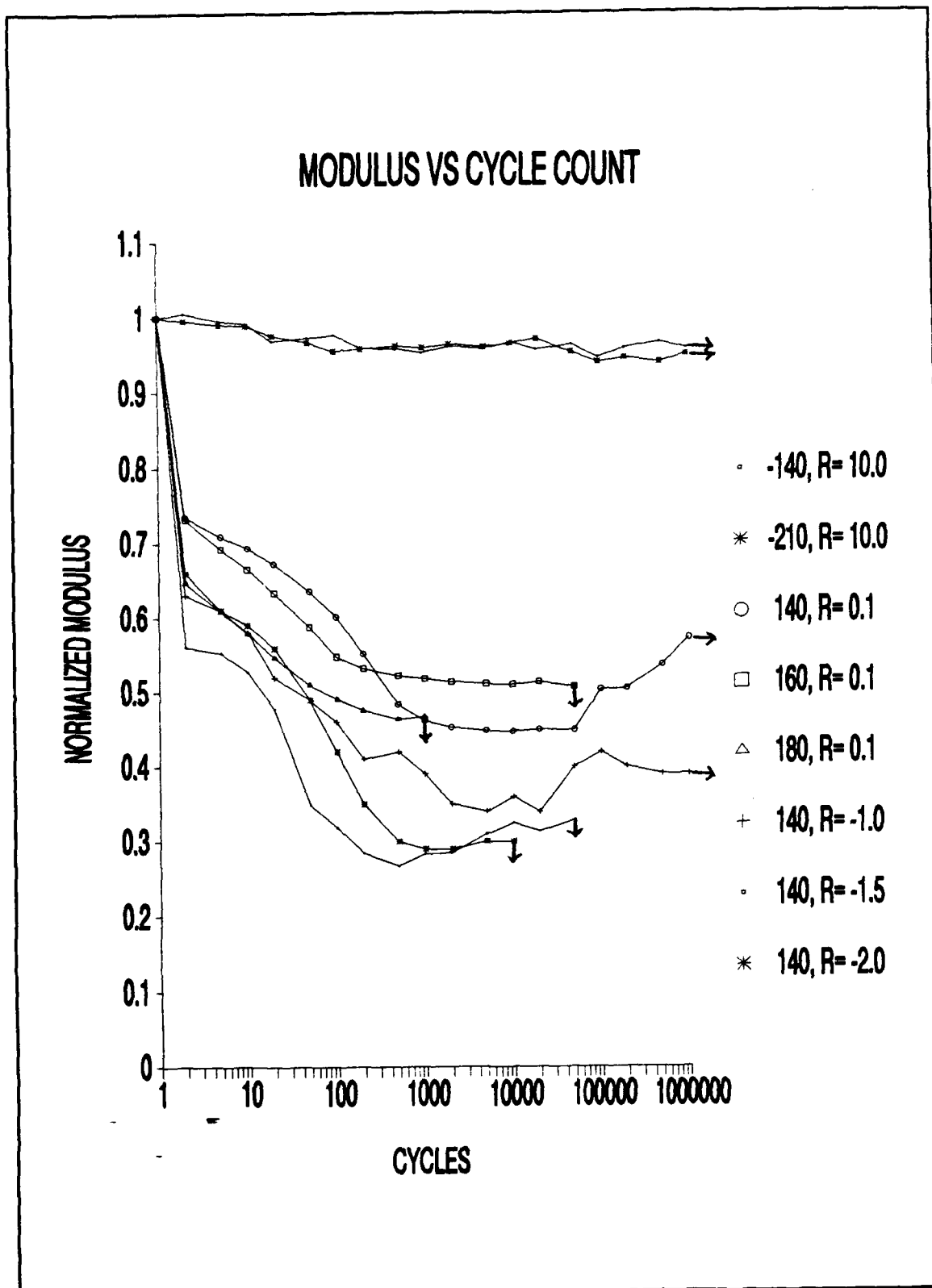
Figure 36
(Normalized Modulus vs Cycles)

of different sizes. In the Appendix, a Fortran program is shown which was used to calculate the area under the stress-strain curves recorded during the fatigue testing. This program basically breaks the curve into a series of trapezoids and the area of each is calculated and then summed together.

Figure 37 shows the energy value calculated with respect to cycles from the stress-strain curves for the tension-tension tests using the above Fortran program.

Just like in the modulus versus cycle count figures, the largest energy value appears during the first cycle, thus confirming that the greatest amount of damage takes place initially regardless of the number of cycles through which the specimen is eventually cycled. What this energy value chart does provide is a better prediction of when/if failure will occur.
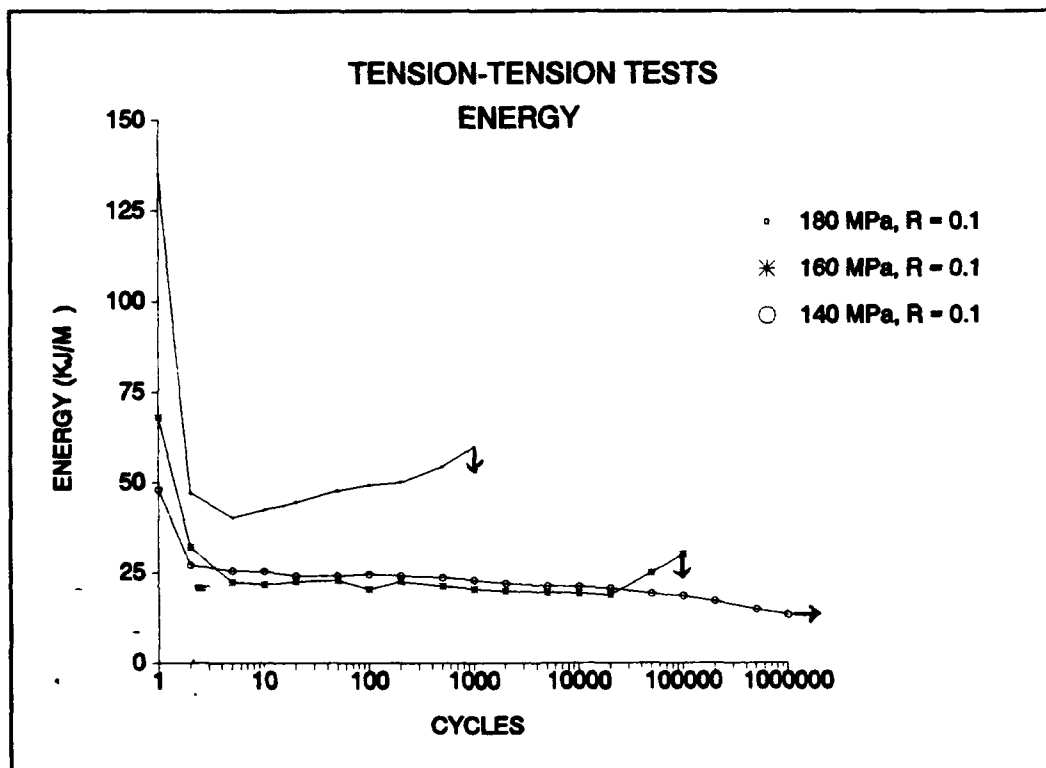

Figure 37
(Tension-Tension Tests, Energy vs Cycles)

The exact point when failure will occur still cannot be readily deduced from this chart, but an increasing energy value is most likely a good indicator that specimen damage is increasing. The magnitude cf the tensile load appears to determine when that energy value begins increasing, with the higher loading producing a larger energy value sooner than the lower loading.

Having viewed the modulus degradation and energy values for the tension-tension tests, the tension-compression tests are the next step. Figure 38 shows the energy value versus cycles for the tension-compression tests.
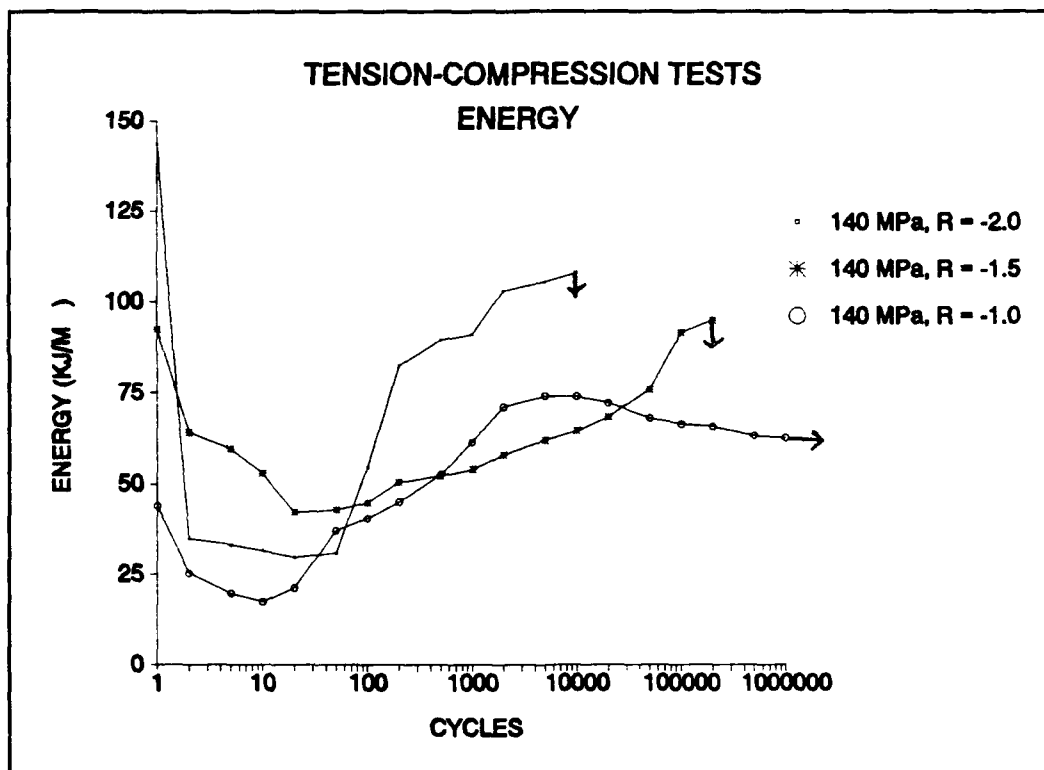

Figure 38
(Tension-Compression Tests, Energy vs Cycles)

It should be noted here that the energy values calculated for the compression-compression tests were orders of magnitude smaller, nearly zero in ¬ome cases, as compared to the tension-tension or tension-compression tests, again confirming that the compression cycles by

46

themselves caused minimal, if any, damage. The average energy per cycle in a compression-compression test was approximately 300 J/m^3 as compared to up to 150,000 J/m^3 in other tests.

While not quite as smooth as the energy curves for the tension-tension tests, these tension-compression curves still provide reasonable data. One observation is that while the energy value starts at a certain level and then immediately decreases, that energy value does level off and then start increasing. This can be explained by the theory that the initial damage is the same as that in the tension-tension tests -- the failure of the 90° plies. The increase in energy must be caused by additional damage not present in the tension-tension tests.

Since all three tension-compression specimens developed longitudinal cracks, this energy increase must be due to internal damage which would eventually cause these longitudinal cracks to appear. This could be weakening of the fiber/matrix bonds, damage to the ply interfaces, internal crack growth, or a combination of each.

What is noticeable is that the increase in energy value occurs much sooner than the appearance of the longitudinal cracks, always within the first hundred cycles; therefore, the development of the longitudinal cracks must be the overall result of previous specimen internal damage which has eventually reached surface level.

V. Conclusions

In summary, the purpose of this study was to determine the fatigue effects that tension-compression cycling would produce in a cross-ply $[0/90]_{2S}$ Nicalon/CAS ceramic matrix composite. The behavior of the Nicalon/CAS composite was determined for static tension and static compression loading. The maximum stress in which 1,000,000 cycles would be reached under tension-tension testing was found. The effect of compression-compression cycling was then investigated, and finally the overall effect of tension-compression loading was determined.

The ultimate strength in tension was found to be 275 MPa. Two noticeable "bends" in the stress-strain curve existed. The first, at 50 MPa, corresponded with failure of the matrix in the 90° plies. The second "bend," at 150 MPa, corresponded with an increase in the transverse crack density in the matrix in both the 0° and 90° plies.

The ultimate strength in compression was found to be 504 MPa. The stress-strain curve was linear to failure with no visible signs of matrix cracking.

In the tension-tension case, the maximum stress for which cycle runout would occur was found to be 140 MPa. Tests conducted above this value (160 MPa, 180 MPa) failed before reaching 1,000,000 cycles while tests conducted at this level achieved cycle runout. In all cases, transverse cracks developed initially in the 90° plies. For specimens which failed, these transverse cracks had spread into the 0° plies and a substantial crack density increase in these plys occurred. Specimens which did not fail exhibited no significant increase in the crack density in the 0° plies.

In the compression-compression tests, no cracks were detected, thus indicating that pure compression loading did not inflict any serious specimen damage. This was verified by the modulus remaining within nirety-five percent of its original value even after 1,000,000 cycles as well as by the hysteretic energy density being almost zero.

In the tension-compression case, the addition of the compression cycles resulted in development of longitudinal cracks parallel to the loading direction which subsequently allowed individual plies to begin buckling and ultimately lead to total specimen failure in the compression cycle. The larger the magnitude of the compression cycle, the earlier the development of longitudinal cracks occurred and, consequently, the earlier failure occurred.

In all tests, recording stress-strain curves and then calculating an elastic modulus was a reasonable indicator that damage had occurred but was not useful in predicting when failure would occur. In the tension-tension cases, the modulus dropped to approximately fifty percent of its original value regardless of whether or not the specimen failed. Similarly, in the tension-compression cases, the modulus dropped to approximately thirty-five percent of its original value regardless of whether or not failure occurred. This additional drop in modulus is most likely attributable to the damage caused by the development of the longitudinal cracks which did not occur in the tension-tension cases.

Calculating the area under the stress-strain curves (energy/volume) seemed to verify the damage that the modulus calculation indicated but also enabled a more educated estimate that the specimen would fail when that energy value began increasing instead of levelling off or decreasing. In all cases, the hysteretic energy density was increasing prior to specimen failure while this density was either steady or decreasing for those specimens in which failure did not occur.

Overall, tension-compression fatigue loading results in increased specimen damage as compared to pure tension-tension or compression-compression loading and can significantly reduce the fatigue life of a cross-ply Nicalon/Calcium-Aluminosilicate ceramic matrix composite.

VI. Recommendations

With the room-temperature fatigue behavior of $[0/90]_{2S}$ well known, the next logical step would be to determine what effects tension-tension and tension-compression tests at elevated temperatures would produce. Since a key feature of ceramic composites is their supposed ability to withstand higher temperatures, verification of this would most likely prove extremely beneficial.

Another potential study would be to determine the threshold at which tension-compression cycles produce no ill effects. This could involve either using the 140 MPa maximum stress value and lowering the R value, or lowering the maximum stress value and increasing the R value. Similarly, this could also be done at elevated temperature.

Finally, thermal-mechanical fatigue (TMF) is another distinct possibility. Since constant room-temperature behavior is known, the effects of in-phase and out-of-phase thermal loads could produce potentially unique behavior.

Bibliography

1.   Rousseau, C.Q., "Monotonic and Cyclic Behavior of SiC/Calcium-Aluminosilicate Ceramic Composite,"in Symposium on Thermal and Mechanical Behavior of Ceramic and Metal Matrix Composites ASTM STP 1080, Kennedy, J.M., Moeller, H.H., and Johnson, W.S., eds, American Society for Testing and Materials, Philadelphia, PA, 1990

2.   Mall, S., Fink, W.E., and Kim, R.Y., "Mechanical behavior of a fiber reinforced ceramic composite under off-axis loading," Advanced Composite Materials, Vol 2, No 2, 1992

3.   Mall, S, and Kim, R.Y., "Failure Mechanisms in Laminates of Silicon Carbide/Calcium-Aluminosilicate Ceramic Composite," in Composites, Vol 23, No 4, July 1992

4.   Zawada, L.P., Butkus, L.M., and Hartman, G., "Tensile and Fatigue Behavior of Silicon Carbide Fiber-Reinforced Aluminosilicate Glass," Journal of the American Ceramic Society, Vol 74, No 11, November 1991, p 2851 - 2858

5.   Wang, S.-W., and Parvizi-Majidi, A., "Mechanical Behavior of Nicalon Fiber-Reinforced Calcium Aluminosilicate Matrix Composites," Ceramic Engineering Scientific Proceedings, 11 [9-10] 1607 - 1616, 1990

6.   Highsmith, A.L., Stinchcomb, W.W., and Reifsnider, K.L., "Effect of Fatigue-Induced Defects on the Residual Response of Composite Laminates," Effects of Defects in Composite Materials, ASTM STP 836, American Society for Testing and Materials, 1984, p 194 - 216

7.   Zawada, L.P., and Pernot, J.J., "Effects of Load Ratio on the Fatigue Behavior of Ceramic Matrix Composites," presented at American Ceramic Society 94th Annual Meeting, 14 April 1992, Minneapolis, Minnesota

8.   Agarwal, Bhagwan D. and Broutman, Lawrence J., Analysis and Performance of Fiber Composites, 2nd Ed., John Wiley & Sons, New York, 1990

9.   Jones, R.M., Mechanics of Composite Materials, Hemisphere Publishing Company, New York, 1975

10.   Tracy, G.D., Failure Mechanisms in a Quasi-Isotropic Ceramic Composite Laminate Under Tensile Fatigue Loading, MS Thesis, AFIT/GAE/ENY/90D-30, School of Engineering, Air Force Institute of Technology (AU), Wright-Patterson AFB, Ohio, December 1990

11. Moschelle, W.R., Fatigue Behavior and Failure Mechanisms of Centrally Notched [0]$_8$ and [(0/90)$_2$]$_s$ Silicon Carbide Reinforced Aluminosilicate Glass, MS Thesis, AFIT/GAE/ENY/91D, School of Engineering, Air Force Institute of Technology (AU), Wright-Patterson AFB, Ohio, December 1991

12.   Tsai Stephen W., Composites Design, Think Composites, Ohio, 1987

13.   Mall, S., and Bachmann, S.E., Transverse Cracking in a Fiber Reinforced Ceramic Matrix Composite, Not Yet Published

14. Talreja, R., "Fatigue of Fibre-Reinforced Ceramics," Proceedings of the 11th Riso International Symposium on Metallurgy and Materials Science: 'Structural Ceramics - Processing, Microstructure and Properties,', Denmark, 1990

15.   Zawada, L.P., Materials Directorate, Wright Laboratory, Wright-Patterson AFB, OH, Personal Communication, September 1992

16.   Rotem, A. & Nelson, H.G., "Failure of a Laminated Composite Under Tension-Compression Fatigue Loading," in Composites Science and Technology, 36 (1989) p 45-62

17. Zawada, L.P. and Pernot, J.J., "Effects of Load Ratio on the Fatigue Behavior of Ceramic Matrix Composites," to be published in the Journal of the American Ceramic Society
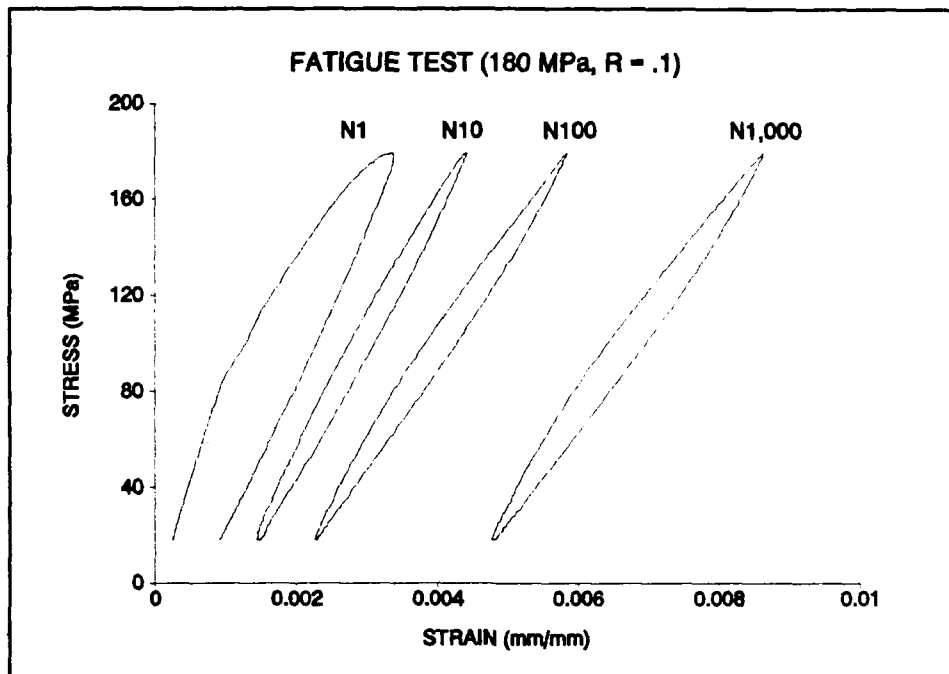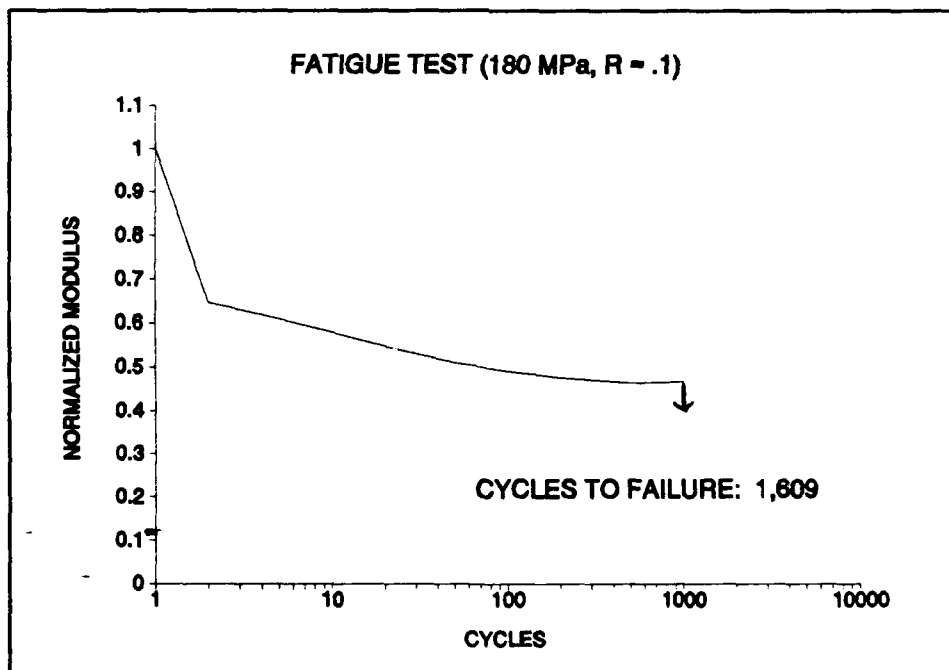
Figure 39
(180 MPa Tension-Tension Test, R = 0.1)

Figure 40
(180 MPa Tension-Tension Test, R = 0.1,
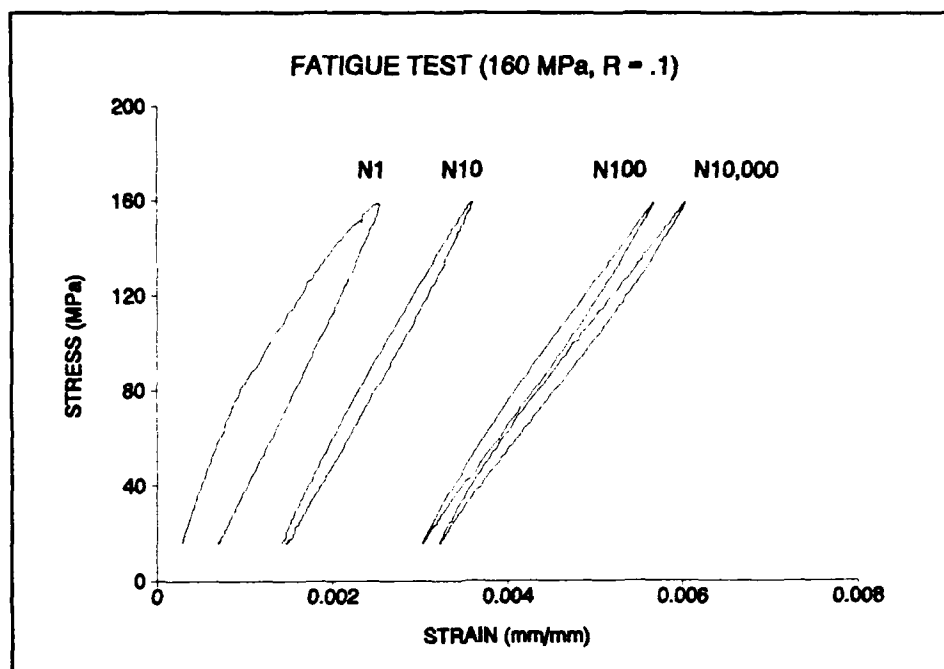Normalized Modulus vs Cycles)

53

Figure 41
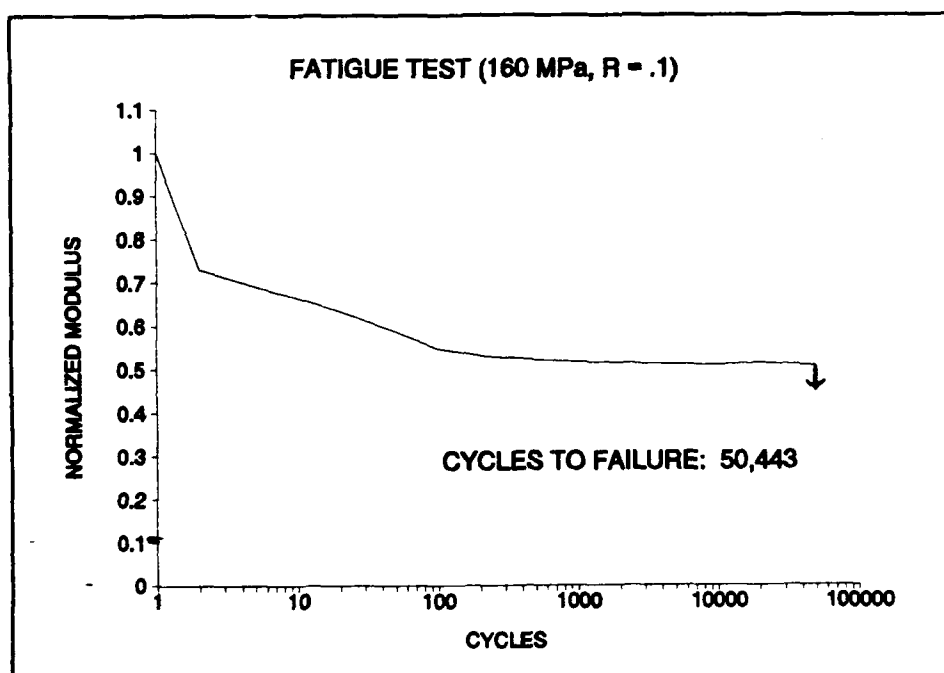(160 MPa Tension-Tension Test, R = 0.1)

Figure 42
(160 MPa Tension-Tension Test, R = 0.1,
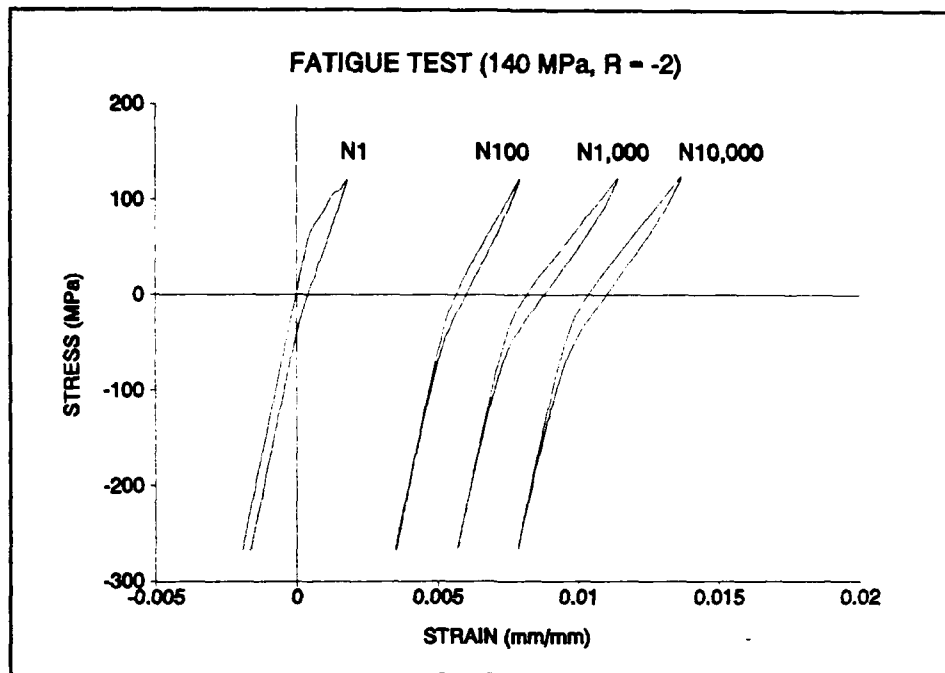Normalized Modulus vs Cycles)

Figure 43
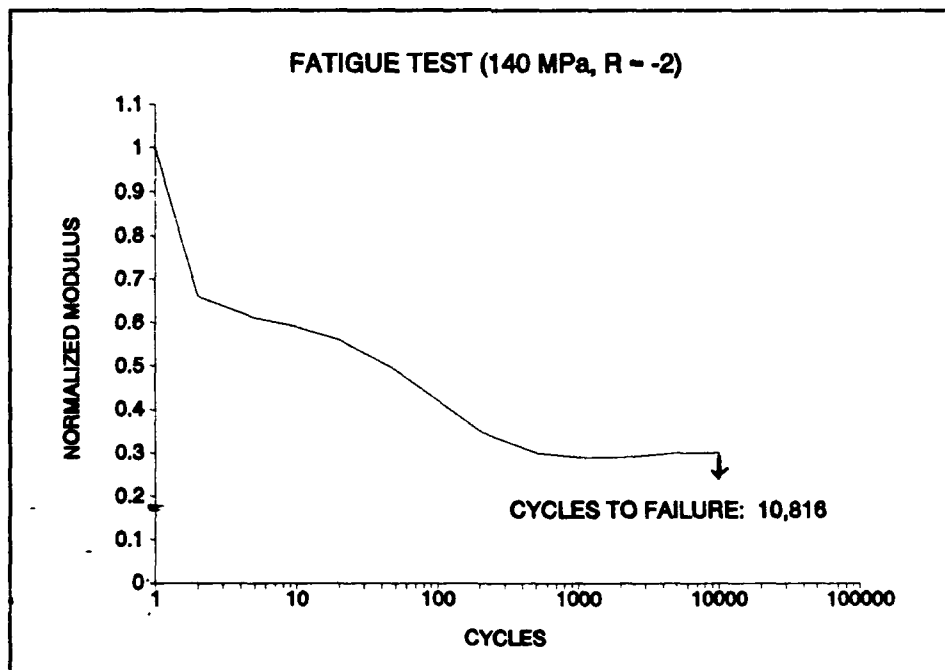(140 MPa Tension-Compression Test, R = -2.0)

Figure 44
(140 MPa Tension-Compression Test, R = -2.0,
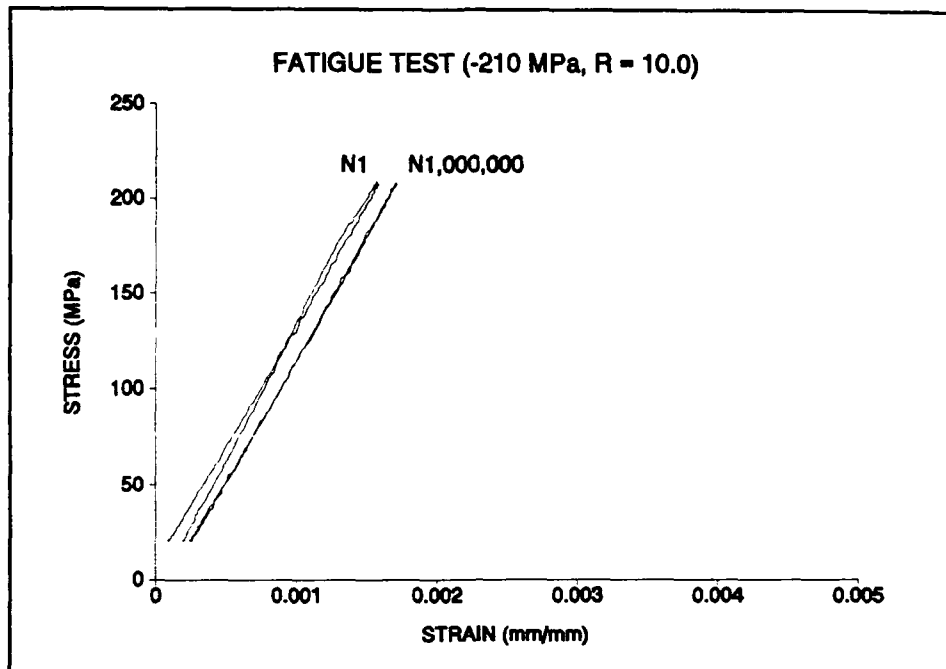Normalized Modulus vs Cycles)

Figure 45
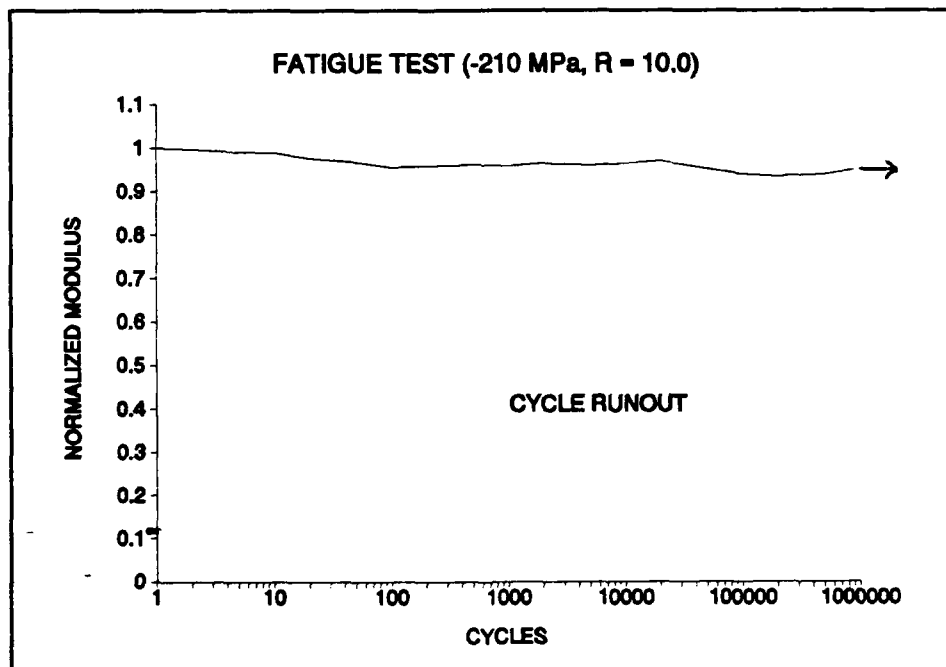(210 MPa Compression-Compression Test, R = 10.0)

Figure 46
(210 MPa Compression-Compression Test, R = 10.0,
Normalized Modulus vs Cycles)

56

Energy Calculation Program

```fortran
      REAL*4 STRESS, STRAIN, KIPS, DISP, SUM, BOX
      DIMENSION STRESS(2000), STRAIN(2000)
      OPEN (7, FILE='ENERGY.IN')
      READ (7,20) AREA
20    FORMAT (F5.4)
      N = 0
      SUM = 0.0
      STRESS(0) = 0.0
      STRAIN(0) = 0.0
      DO 5 I = 1, 1000
      READ (7,10) KIPS, DISP
10    FORMAT (2X,E11.5,2X,E11.5)
      STRAIN(I) = DISP / .3
      STRESS(I) = ((KIPS * 1000. / AREA) * 6895.)
      N = I - 1
      SUM = SUM + ((STRESS(I) + STRESS(N))/2. * (STRAIN(I) - STRAIN(N)))
5     CONTINUE
      SUM = SUM - (STRESS(1)/2. * STRAIN(1))
      BOX = (STRESS(1000) + STRESS(1)) / 2. * (STRAIN(1000) - STRAIN(1))
      SUM = (SUM - BOX)
      WRITE(*,25) SUM
25    FORMAT (5X, F12.0)
      CLOSE (7)
      STOP
      END
```

Vita

Captain Frank A. Opalski was born on 27 December 1964 in Wilkes-Barre, Pennsylvania. He graduated from West Morris Mendham High School in Mendham, New Jersey, in 1982. He then attended Rutgers, the State University of New Jersey, from 1982 through 1986 and graduated with a Bachelor of Science Degree in Mechanical Engineering. He joined the Air Force, attended Officer Training School (OTS), and was commissioned on 12 December 1986.

Captain Opalski's military assignments include successfully completing Specialized Undergraduate Navigator Training (SUNT) and Electronic Warfare Officer (EWO) training at Mather AFB, California; B-52G initial qualification training at Castle AFB, California; operational B-52G electronic warfare officer at Wurtsmith AFB, Michigan; and logistics engineer in the Short Range Attack Missile II (SRAM II) System Program Office (SPO) at Wright-Patterson AFB, Ohio.

Captain Opalski entered the *School of Engineering*, Air Force Institute of Technology, in May 1991.

REPORT DOCUMENTATION PAGE

1. AGENCY USE ONLY (Leave blank)	2. REPORT DATE December 1992	3. REPORT TYPE AND DATES COVERED Master's Thesis

4. TITLE AND SUBTITLE	5. FUNDING NUMBERS
FATIGUE BEHAVIOR OF A CROSS-PLY CERAMIC MATRIX COMPOSITE UNDER TENSION-TENSION AND TENSION-COMPRESSION LOADING	

6. AUTHOR(S)

7. PERFORMING ORGANIZATION NAME(S) AND ADDRESS(ES)	8. PERFORMING ORGANIZATION REPORT NUMBER
Air Force Institute of Technology, WPAFB, OH 45433	AFIT/GAE/ENY/92D-02

9. SPONSORING MONITORING AGENCY NAME(S) AND ADDRESS(ES)	10. SPONSORING MONITORING AGENCY REPORT NUMBER
Dr. Walter F. Jones AFOSR/NA Bolling AFB, DC 20322-6448	

11. SUPPLEMENTARY NOTES

12a. DISTRIBUTION / AVAILABILITY STATEMENT	12b. DISTRIBUTION CODE
Approved for public release; distribution unlimited	

13. ABSTRACT (Maximum 200 words)

A study was conducted which investigated the behavior of a cross-ply ($[0/90]_{2s}$) Nicalon/Calcium-Aluminosilicate (Nicalon/CAS) ceramic matrix composite at room temperature under tension-compression fatigue loading. Material behavior and damage was recorded by stress-strain curves, elastic modulus, hysteretic energy density, and acetate replication techniques. Tension-tension fatigue tests at a load ratio R of 0.1 ($R = \sigma_{min}/\sigma_{max}$) were completed which determined that 140 MPa was the maximum stress allowable in which cycle runout (1,000,000 cycles) would occur. Above this value, transverse crack density increased with respect to cycles and failure ultimately occurred. Tension-compression tests were then performed at load ratios of -2.0, -1.5, and -1.0 with 140 MPa as the maximum tensile stress. In all cases, longitudinal cracks parallel to the loading direction developed. The greater the magnitude of the compressive load, the sooner these longitudinal cracks appeared. Failure always occurred in compression due to buckling of individual plies, thus indicating that tension-compression can significantly reduce fatigue life. Using the elastic modulus as a means of verifying damage was acceptable, but it did not reasonably predict specimen failure. On the other hand, the area under the stress-strain curve (hysteretic energy density) was a better indicator of probable failure since specimens which achieved cycle runout showed either a decreasing or constant energy density while those which failed always showed an increasing value.

14. SUBJECT TERMS		15. NUMBER OF PAGES
Ceramic Matrix Composite, Tension-Tension Fatigue, Hysteretic Energy Density, Tension-Compression Fatigue		58
		16. PRICE CODE

17. SECURITY CLASSIFICATION OF REPORT	18. SECURITY CLASSIFICATION OF THIS PAGE	19. SECURITY CLASSIFICATION OF ABSTRACT	20. LIMITATION OF ABSTRACT
Unclassified	Unclassified	Unclassified	UL

NSN 7540-01-280-5500

Standard Form 298 (Rev. 2-89)
Prescribed by ANSI Std. Z39-18
298-102